Protonation of Ferrous Dinitrogen Complexes Containing a Diphosphine Ligand with a Pendent Amine

Zachariah M. Heiden,[‡] Shentan Chen,[‡] Michael T. Mock,[‡,*] William G. Dougherty,[†] W. Scott Kassel,[†] Roger Rousseau,[‡] and R. Morris Bullock[‡]

[‡]Center for Molecular Electrocatalysis, Physical Sciences Division, Pacific Northwest National Laboratory, Richland, Washington 99352, United States

[†]Department of Chemistry, Villanova University, Villanova, Pennsylvania 19085, United States

Ⓢ Supporting Information

ABSTRACT: The addition of acids to ferrous dinitrogen complexes $[FeX(N_2)(P^{Et}N^{Me}P^{Et})(dmpm)]^+$ (X = H, Cl, or Br; $P^{Et}N^{Me}P^{Et}$ = $Et_2PCH_2N(Me)CH_2PEt_2$; and dmpm = $Me_2PCH_2PMe_2$) gives protonation at the pendent amine of the diphosphine ligand rather than at the dinitrogen ligand. This protonation increased the ν_{N2} band of the complex by 25 cm^{-1} and shifted the Fe(II/I) couple by 0.33 V to a more positive potential. A similar IR shift and a slightly smaller shift of the Fe(II/I) couple (0.23 V) was observed for the related carbonyl complex $[FeH(CO)(P^{Et}N^{Me}P^{Et})(dmpm)]^+$. $[FeH(P^{Et}N^{Me}P^{Et})-(dmpm)]^+$ was found to bind N_2 about three times more strongly than NH_3. Computational analysis showed that coordination of N_2 to Fe(II) centers increases the basicity of N_2 (vs free N_2) by 13 and 20 pK_a units for the trans halides and hydrides, respectively. Although the iron center increases the basicity of the bound N_2 ligand, the coordinated N_2 is not sufficiently basic to be protonated. In the case of ferrous dinitrogen complexes containing a pendent methylamine, the amine site was determined to be the most basic site by 30 pK_a units compared to the N_2 ligand. The chemical reduction of these ferrous dinitrogen complexes was performed in an attempt to increase the basicity of the N_2 ligand enough to promote proton transfer from the pendent amine to the N_2 ligand. Instead of isolating a reduced Fe(0)−N_2 complex, the reduction resulted in isolation and characterization of $HFe(Et_2PC(H)N(Me)CH_2PEt_2)(P^{Et}N^{Me}P^{Et})$, the product of oxidative addition of the methylene C−H bond of the $P^{Et}N^{Me}P^{Et}$ ligand to Fe.
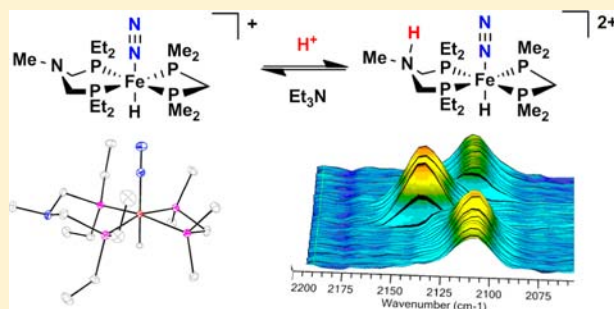
■ INTRODUCTION

The development of homogeneous transition metal complexes for the reduction and/or functionalization of N_2 has been an area of research for more than 40 years.[1] Iron complexes have been targeted[2] for N_2 reduction studies because iron is an abundant, inexpensive,[3] and biorelevant transition metal found in the active site of the nitrogenase metalloenzyme. The active site of nitrogenase contains two Fe_4S_3 cubane units connected through a carbide and three sulfide linkers (Figure 1), where one of the metal atoms (designated M in Figure 1) can be Mo, V, or Fe.[4]
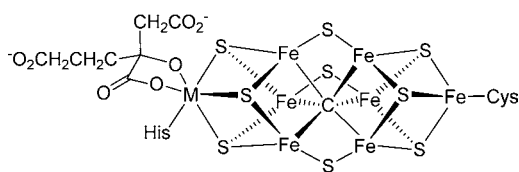

Figure 1. Proposed active site of nitrogenase, where M can be Fe, Mo, or V.

The nitrogenase metalloenzyme reduces N_2 using a combination of *protons* and *electrons* at ambient temperature and pressure to generate ammonia.[5] The N_2 reduction pathway requires eight protons and eight electrons, producing one hydrogen molecule and two ammonia molecules; a comprehensive understanding of the N_2 reduction mechanism has been sought for over three decades.[6] Recent spectroscopic studies on the FeMo cofactor from the groups of Hoffman and Seefeldt suggest N_2 reduction occurs by an "alternating" reduction pathway (symmetric pathway in Scheme 1), where N_2 is reduced stepwise, with protonation occurring first at the distal N atom followed by protonation at the proximal N atom, possibly involving multiple iron centers in oxidation states common to biological systems (e.g., Fe^{II} and/or Fe^{III}; Scheme 1).[6b,7] Importantly, these findings encourage the development of synthetic systems to both replicate and understand the factors that govern N_2 binding, elucidate the mechanism of reduction pathways, and examine the protonated N_2 intermediates along the reduction pathway.

Scheme 1. Possible N₂ Reduction Pathways with Iron
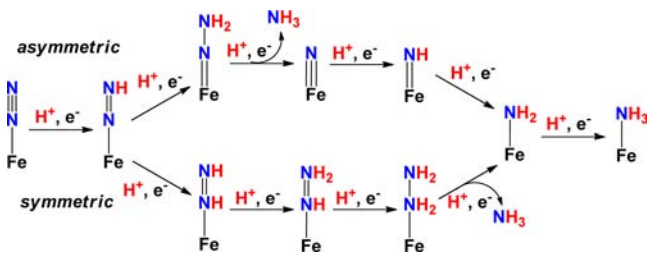
To date, two types of coordination complexes have been shown to catalytically reduce N₂ to NH₃ with *protons* and *electrons*. In contrast to nitrogenase, these coordination complexes are proposed to undergo an asymmetric reduction of N₂ to NH₃ (Scheme 1), where protonation occurs first at the distal nitrogen atom, followed by NH₃ expulsion, prior to protonation of the proximal nitrogen atom. Schrock's Mo triamidoamine catalyst has been shown to produce eight equivalents of NH₃ (four turnovers).[8] In a recent example by Nishibayashi et al., a Mo catalyst supported by a phosphine-based pincer ligand was shown to produce 23 equivalents of NH₃ (12 catalyst turnovers).[9] Although these two Mo-based complexes catalyze the reduction of N₂ to ammonia, only stoichiometric ammonia formation has been demonstrated with iron-based complexes.[10] The stoichiometric production of ammonia and hydrazine in yields ranging from 4 to 82% has been reported using Fe^{II},[11] Fe^{I},[12] and Fe^{0} dinitrogen[13] and iron-nitride complexes.[14] Peters and co-workers expanded upon this previous work by demonstrating that upon the addition of an external reductant, N₂H₄ generation can be increased from 17 to 47%.[15]

Biological enzymes hydrogenase and nitrogenase have been found to employ pendent bases (histidine-195 in the case of nitrogenase),[7e,16] or proton channels,[5a,17] to promote the activation/production of H₂ and N₂, through proton-coupled-electron-transfer (PCET) reactions.[18] One way to design a molecular catalyst to promote PCET reactions is by the incorporation of pendent amines that function as proton relays, in the second coordination sphere of the ligand. This concept has been previously employed in the electrochemical reduction of protons to H₂ in diphosphine supported Ni catalysts,[19] and in the reduction of dioxygen.[20] Recognizing that protonation of the pendent amine groups can modulate the redox potential of the complex and appreciating the importance of controlling proton movement in these multiproton, multielectron reactions, we sought to explore the effect of pendent amines as proton relays on the coordination of N₂ and its subsequent protonation,[21] with the ultimate goal of catalytic reduction of N₂ to NH₃.

Herein, we report the synthesis of ferrous dinitrogen complexes of the type [FeX(N₂)($P^{Et}N^{Me}P^{Et}$)(dmpm)]⁺ (X = H, Cl, or Br; $P^{Et}N^{Me}P^{Et}$ = Et₂PCH₂N(Me)CH₂PEt₂; and dmpm = Me₂PCH₂PMe₂), which introduces a basic pendent amine site in the phosphine ligand backbone. In this investigation, we study the reaction of the Fe(N₂) complexes with acid and examine the effects of protonation with regard to N₂ ligand binding and redox behavior. We complement these experimental results with a computational study to provide a quantitative comparison of the basicity of the Fe-bound N₂ and the pendent amine. In addition, N₂ ligand substitution by NH₃ and H₂ is examined, and initial efforts to prepare Fe^{0}-N₂ complexes with the $P^{Et}N^{Me}P^{Et}$ ligand are described.

■ RESULTS AND DISCUSSION

Synthesis and Characterization of Ferrous N₂ Complexes. To assess whether the introduction of a proton relay in the ligand of a ferrous dinitrogen complex aids in N₂ binding and subsequent reduction to ammonia, we synthesized complexes of the type [FeX(N₂)($P^{Et}N^{Me}P^{Et}$)(dmpm)]⁺ (X = H, Cl, or Br; $P^{Et}N^{Me}P^{Et}$ = Et₂PCH₂N(Me)CH₂PEt₂; and dmpm = Me₂PCH₂PMe₂; see Figure 2). The $P^{Et}N^{Me}P^{Et}$ ligand was
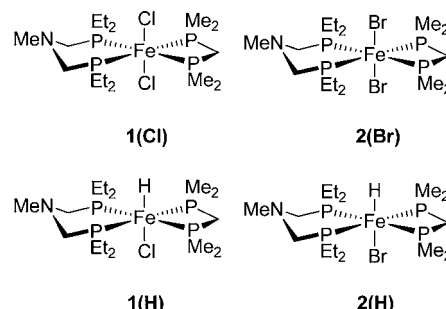

Figure 2. Ferrous complexes containing pendent amines used in the synthesis of Fe–N₂ complexes.

chosen to allow for the direct comparison of N₂ chemistry to the previously reported H₂ chemistry, [FeH(H₂)($P^{Et}N^{Me}P^{Et}$)(dmpm)]⁺.[22] Incorporation of only one pendent amine allowed for an easier comparison to previously reported ferrous dinitrogen complexes.[2] The dinitrogen complex was prepared as shown in eq 1. The iron chloride complexes
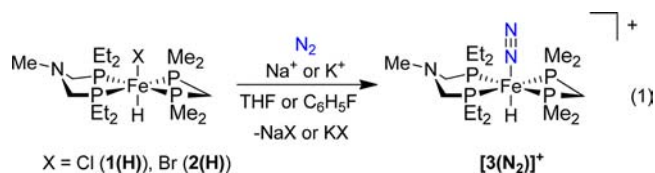
FeCl₂($P^{Et}N^{Me}P^{Et}$)(dmpm) (**1(Cl)**) and FeHCl($P^{Et}N^{Me}P^{Et}$)(dmpm) (**1(H)**) have been previously reported by DuBois and co-workers,[22a] and iron bromide FeBr₂($P^{Et}N^{Me}P^{Et}$)(dmpm) (**2(Br)**) and FeHBr($P^{Et}N^{Me}P^{Et}$)(dmpm) (**2(H)**) are reported herein. FeHBr($P^{Et}N^{Me}P^{Et}$)(dmpm) was prepared following the synthetic method reported for FeHCl($P^{Et}N^{Me}P^{Et}$)(dmpm),[22a] by the addition of Bu₄NBH₄ to FeBr₂($P^{Et}N^{Me}P^{Et}$)(dmpm) in THF at −35 °C, and was isolated in 48% yield.

Ferrous dinitrogen complexes were synthesized via abstraction of a halide from the parent dihalide and hydrido-halide complexes. The N₂-hydride complex *trans*-[FeH(N₂)($P^{Et}N^{Me}P^{Et}$)(dmpm)]⁺ ([**3(N₂)**]⁺) can be prepared by halide abstraction from FeHCl($P^{Et}N^{Me}P^{Et}$)(dmpm) (**1(H)**) or FeHBr($P^{Et}N^{Me}P^{Et}$)(dmpm) (**2(H)**) using salts containing noncoordinating anions: NaBPh₄, KB(C₆F₅)₄, or NaBAr^F₄ (Ar^F = 3,5-bis(trifluoromethyl)phenyl) in 60−75% yield (eq 1). The reaction of **1(H)** or **2(H)** with NaBPh₄ in THF yielded [**3(N₂)**]⁺ in ~2.5 h as monitored by *in situ* IR spectroscopy (Figure 3) and ³¹P NMR spectroscopy. [**3(N₂)**]**BPh₄** exhibits a ν_{NN} band at 2095 cm⁻¹ (KBr; 2103 cm⁻¹ in THF) and a ν_{FeH} band at 1886 cm⁻¹ (KBr). The measured vibrational frequencies of [**3(N₂)**]**BPh₄** are similar to the values previously reported for *trans*-[FeH(N₂)(dmpe)₂]BPh₄ (dmpe = Me₂PCH₂CH₂PMe₂; ν_{NN} = 2094 cm⁻¹, ν_{FeH} = 1841 cm⁻¹ (ethanol))[23] and [FeH(N₂)((P(C₃H₆OMe)₂CH₂)₂)₂]BPh₄
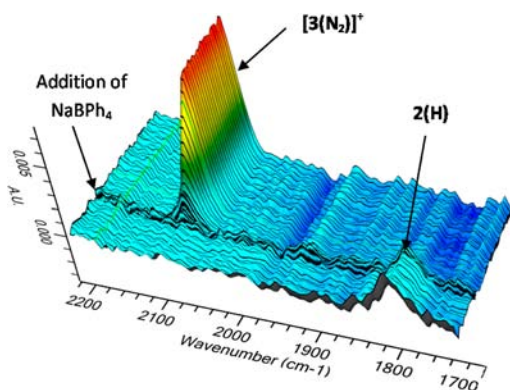
4027

dx.doi.org/10.1021/ic4000704 | *Inorg. Chem.* 2013, 52, 4026−4039

Figure 3. In situ infrared spectra versus time, monitoring the formation of $[3(N_2)]^+$ (ν_{NN} = 2103 cm^{-1}) from the halide abstraction of $1(H)$ (ν_{FeH} = 1816 cm^{-1}) with NaBPh$_4$ in THF over 4 h.

(ν_{NN} = 2088 cm^{-1} (KBr)).[24] The ^{31}P NMR spectrum of $[3(N_2)]^+$ contains two multiplets of an AA′XX′ pattern at δ 38.9 and −0.1, assigned as the P^{Et}N^{Me}P^{Et} and dmpm resonances, respectively. The hydride resonance in the ^{1}H NMR spectrum appears as a multiplet at δ −14.6, which is about 13 ppm downfield from the hydride resonance of $1(H)$ or $2(H)$. Reactions to prepare $[3(N_2)]^+$ performed in fluorobenzene, employing KB(C$_6$F$_5$)$_4$ or NaBAr$^F_4$ as a halide abstraction agent, were considerably faster than in THF and reached completion within seconds. Experiments performed using ^{15}N$_2$ resulted in the expected shift of the ν_{NN} band to 60 cm^{-1} lower frequency, appearing at 2054 cm^{-1} (fluorobenzene). The ^{15}N NMR spectrum (THF-d_8) exhibits two resonances at δ −41.8 and δ −59.8 vs CH$_3$NO$_2$, assigned as the distal and proximal nitrogen atoms, respectively. Dissolution of this complex in fluorobenzene under ambient ^{14}N$_2$ atmosphere resulted in complete exchange of the ^{15}N$_2$ label for ^{14}N$_2$ over the course of ~2 h.

Vapor diffusion of pentane into a fluorobenzene solution of $[3(N_2)]B(C_6F_5)_4$ produced yellow X-ray quality crystals in 60% yield. The molecular structure, shown in Figure 4, reveals a slightly distorted octahedral Fe(II) cation with the P^{Et}N^{Me}P^{Et} and dmpm ligands in the equatorial plane. The P3–Fe–P4 angle of the dmpm ligand is 73.85(14)°, while the P1–Fe–P2
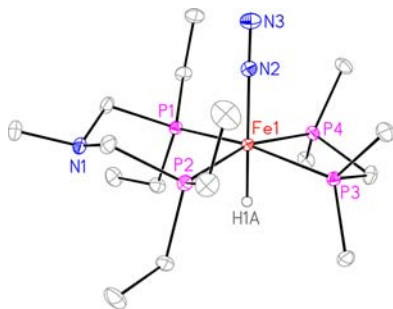

Figure 4. Molecular structure of the cation $[FeH(N_2)(P^{Et}N^{Me}P^{Et})$-$(dmpm)]^+$ ($[3(N_2)]^+$). Thermal ellipsoids are drawn at 30% probability. The hydrogen atoms (except for the Fe–H) are omitted for clarity. Selected bond distances (Å) and angles (deg): P(1)–Fe(1) = 2.214(1), P(2)–Fe(1) = 2.208(1), P(3)–Fe(1) = 2.222(1), P(4)–Fe(1) = 2.219 (1), Fe(1)–N(2) = 1.827(1), Fe(1)–H(1A) = 1.457(18), N(2)–N(3) = 1.109(2), P(2)–Fe(1)–P(1) = 90.73(1), P(3)–Fe(1)–P(4) = 73.85(1), N(2)–Fe(1)–H(1A) = 178.9(7), Fe(1)–N(2)–N(3) = 178.67(12).

angle of the P^{Et}N^{Me}P^{Et} ligand is 90.73(14)°. The average Fe–P bond length for the P^{Et}N^{Me}P^{Et} ligand is 2.211(4) Å, and the average Fe–P bond length for the dmpm ligand is slightly longer at 2.221(4) Å. The hydride ligand trans to the N$_2$ ligand was located from the difference map and exhibits a H–Fe–N(2) angle of 178.9(7)°. The Fe–H and Fe–N$_2$ bond lengths are 1.46(2) Å and 1.827(1) Å, respectively. Values involving the Fe–H bond length should be interpreted cautiously since hydrogen atoms are not located with high accuracy by X-ray diffraction studies.[25] The N(2)–N(3) bond length of the coordinated N$_2$ ligand is 1.109(2) Å. For comparison, $[FeH(N_2)(dmpe)_2]BPh_4$ and $[FeH(N_2)(depe)_2]BPh_4$ have N–N bond lengths of 1.13(3) Å and 1.070(12) Å, respectively.[23,26] In all of these examples, the N$_2$ ligand is considered to be only weakly activated with respect to free N$_2$ (1.0975 Å)[2a] based on N–N bond length and IR stretching frequency, described above. The six-membered ring formed by coordination of the P^{Et}N^{Me}P^{Et} ligand to the Fe center resides in the chair conformation with the pendent amine positioned exo with respect to the N$_2$ ligand (Figure 4).

Halide abstraction from $1(Cl)$ or $2(Br)$ with KB(C$_6$F$_5$)$_4$ in fluorobenzene under an N$_2$ atmosphere resulted in the formation of $[FeCl(N_2)(P^{Et}N^{Me}P^{Et})(dmpm)]^+$ ($[1(N_2)]^+$) or $[FeBr(N_2)(P^{Et}N^{Me}P^{Et})(dmpm)]^+$ ($[2(N_2)]^+$), which contains a ν_{NN} band at 2110 and 2111 cm^{-1}, respectively (eq 2). In
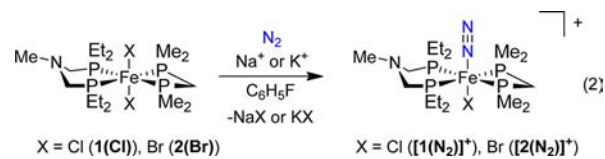
contrast to $[3(N_2)]^+$, the N$_2$ ligand was found to be highly labile.[27] For example, no ν_{NN} band was found in the IR spectrum of the solid product collected in KBr after removing the solvent from $[2(N_2)]^+$ under a vacuum, or if the reaction was undertaken in THF. Crystallization of the reddish-orange solution under an N$_2$ atmosphere yielded a red crystalline product for which the elemental analysis is consistent with a five-coordinate complex without an N$_2$ ligand, $[FeBr$-$(P^{Et}N^{Me}P^{Et})(dmpm)]^+$. Although an X-ray diffraction study of these crystals did not yield a structure of publishable quality, the refined data clearly showed connectivity in the first coordination sphere in which a five-coordinate iron center coordinated to four phosphines and a bromide could be observed. To our knowledge, only two examples of a 5-coordinate Fe complex of this type have been structurally characterized, reported by Tyler et al.[24] and Tuczek et al.[28] $[1(N_2)]^+$ can also be prepared from $1(H)$, by reaction with either Ph$_3$C$^+$ or B(C$_6$F$_5$)$_3$ in chlorobenzene-d_5. However, further attempts to obtain better crystallographic data of $[1(N_2)]^+$ or the five-coordinate iron complex were unsuccessful.

Protonation Studies of [FeH(N$_2$)(P^{Et}N^{Me}P^{Et})(dmpm)]$^+$ ([3(N$_2$)]$^+$). The addition of acids to $[3(N_2)]^+$ was investigated by a combination of ^{1}H, ^{31}P, and ^{15}N NMR spectroscopy and in situ IR experiments. Accordingly, the lability of N$_2$, subsequent decomposition pathways, and IR spectroscopic signature of N$_2$ bound to Fe in the protonated complex were investigated. For the NMR studies, ^{15}N$_2$ was incorporated into $[3(N_2)]^+$, ($[FeH(^{15}N_2)(P^{Et}N^{Me}P^{Et})(dmpm)]BPh_4$), to conveniently acquire ^{15}N NMR spectral data. The addition of one equivalent of triflic acid (HOTf) to $[3(^{15}N_2)]BPh_4$ at −35 °C in THF-d_8
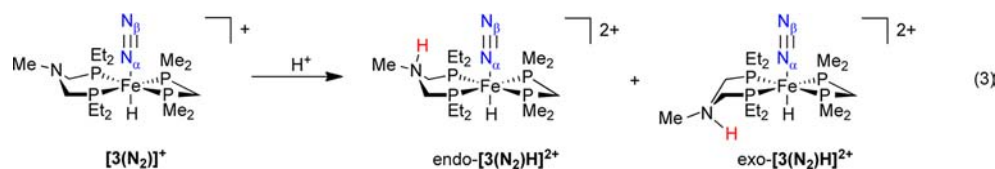
resulted in the protonation of the pendent amine of the $P^{Et}N^{Me}P^{Et}$ ligand and the formation of two protonated isomers (either endo or exo with respect to the N_2 ligand; $[3(^{15}N_2)$-$H]^{2+}$), see eq 3 and Figure 5. Two pairs of multiplets of an
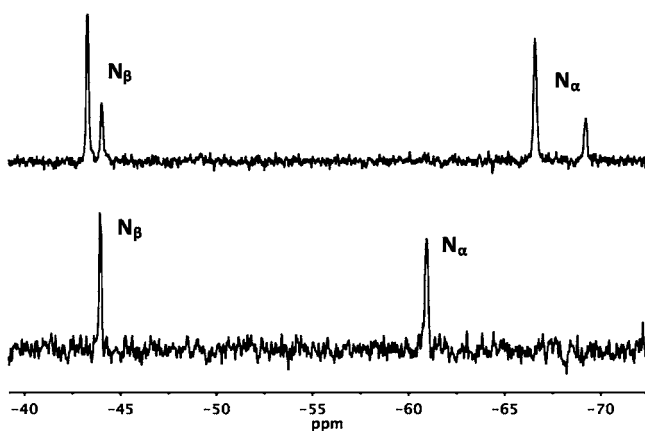

Figure 5. $^{15}N\{^1H\}$ NMR spectra at −35 °C in THF-d_8 of (bottom) $[3(^{15}N_2)]^+$ and (top) $[3(^{15}N_2)]^+$ with one equivalent of HOTf, where N_α = proximal nitrogen atom and N_β = distal nitrogen.

AA′XX′ pattern are observed in the ^{31}P NMR spectrum at δ 47.9, −1.2 and δ 52.8, −0.2 in a ~3:1 ratio, assigned as the $P^{Et}N^{Me}P^{Et}$ and dmpm ligands, respectively. Notable features in the corresponding ^1H NMR spectrum include two pentets corresponding to the hydride ligand at δ −14.62 ($^1J_{HP}$ = 47.6 Hz) and −14.92 ($^1J_{HP}$ = 48.2 Hz) and two broad peaks at δ 9.54 and 9.35 assigned to the NH of the protonated pendent amine for the major and minor product, respectively (see Supporting Information for NMR spectral data). A cross-peak in the $^1H-^{15}N$ correlation experiment (HSQC) confirmed this assignment as the protonated pendent amine with the corresponding ^{15}N NMR shifts at δ −337.3 and −335.9 for the major and minor isomers, respectively. The observed ^{15}N chemical shifts are consistent with values reported for protonated alkyl amines.[29] ^{15}N NMR spectral data also contain two pairs of singlets (four total resonances) in a ~3:1 ratio. The major isomer, at δ −43.3 and −66.5, and the minor species located at δ −44.0 and −69.2 (Figure 5), correspond to the distal (N_β) and proximal (N_α) nitrogen atoms of $^{15}N_2$, respectively. While NMR studies have not established which protonated isomer, exo-$[3(N_2)H]^{2+}$ or endo-$[3(N_2)H]^{2+}$, is the major product (NOESY experiments were inconclusive), it is probable that the major isomer contains the proton on the pendent amine positioned exo with respect to the N_2 ligand (eq 3). This assignment has been corroborated by DFT calculations (see computational section below).

The protonation of $[3(N_2)]^+$ was investigated further by IR spectroscopy. For this experiment, complex $[3(N_2)]B(C_6F_5)_4$ was conveniently generated in situ from $2(H)$ and one equivalent of $KB(C_6F_5)_4$ in fluorobenzene. The reaction, monitored by in situ IR spectroscopy, yielded a ν_{NN} band of $[3(N_2)]B(C_6F_5)_4$ at 2114 cm^{-1}. The addition of one equivalent

of $[H(OEt_2)_2][B(C_6F_5)_4]$ to a solution of $[3(N_2)]^+$ at −40 °C resulted in an immediate increase in the stretching frequency of the ν_{N2} band by 25 cm^{-1} to 2139 cm^{-1}, as shown in Figure 6.
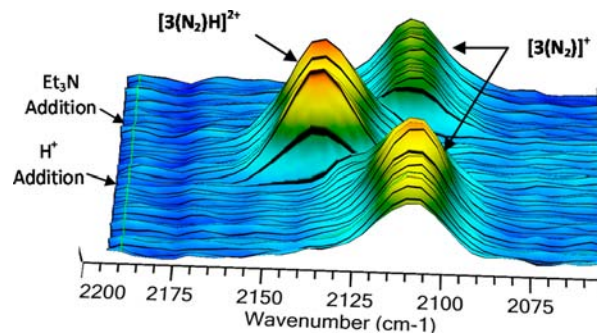

Figure 6. In situ IR plot recorded at −40 °C from the reaction of $[3(N_2)]B(C_6F_5)_4$ with one equivalent of $[H(OEt_2)_2][B(C_6F_5)_4]$ in fluorobenzene followed by the addition of one equivalent of Et_3N. The total reaction time was 50 min (each increment is 1 min).

The complex resulting from protonation of $[3(N_2)]^+$, ($[3(N_2)$-$H]^{2+}$), is stable in solution for over 24 h at −40 °C, and the protonation of $[3(N_2)]^+$ is reversible upon the addition of a base (Et_3N). This is a unique example of a ferrous-N_2 complex, where the shift in the stretching frequency of the ν_{NN} band was a result of directly protonating the ancillary ligand. The observed increase in ν_{N2} stretching frequency indicates that N_2 is not protonated, as a lower energy N_2 band would be expected if that were the case.[30]
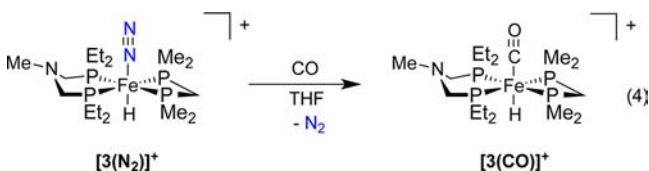
To explain the origin of the increase in the ν_{N2} band, two possibilities are considered: a through bond inductive effect (diminished back-bonding to the N_2 ligand) or an electrostatic effect (due to increased positive charge of the complex). In a related example by Schrock and co-workers, the addition of one equivalent of acid to the molybdenum complex $Mo(N_2)$-$(HIPTN_3N)$ (HIPT = 3,5-$(2,4,6-^iPr_3C_6H_2)_2C_6H_3$), supported by the triamidoamine ligand, generates a protonated product in which the ν_{N2} band shifts 67 cm^{-1}, from 1990 to 2057 cm^{-1}.[31] Their studies suggest that direct protonation of one of three amido groups of the ligand resulted in decreased back-bonding to the dinitrogen ligand, increasing the frequency of the ν_{NN} band. Studies by Sellmann and Sutter reveal an analogous result in the shift of the ν_{CO} band stretching frequency used to probe the electronic effect induced by protonation at the sulfur atom of a bound thiolate donor of the bis-benzene-dithiolate ethylene bridged ligand in $[Fe(CO)_2(MeSC_6H_4SC_2H_4SC_6H_4SMe)]$ or the bis-benzene-dithiolate bis-ethylene-amine bridged ligand in $[Fe(CO)(SC_6H_4SC_2H_4NHC_2H_4SC_6H_4S)]$. In this example, protonation of the thiolate directly bound to the Fe center resulted in an increase of the ν_{CO} bands by ca. 40 cm^{-1}.[5c] The greater magnitude of this shift in stretching frequency observed by Sellmann and Sutter, compared to the smaller difference between $[3(N_2)]^+$ and $[3(N_2)H]^{2+}$, can be attributed to the difference in the through bond proximity of the protonated site to the metal center. In complexes structurally similar to $[3(N_2)]^+$, where the proximity of the protonated group to the

metal center is comparable, smaller carbonyl frequency shifts have been observed. For example, the addition of protons to azadithiolate [FeFe]-hydrogenase model complexes results in a ν_{CO} shift of 15 cm^{-1} independent of the nitrogen substituents or number of phosphines present on the iron centers.[32]

For the protonation of $[3(N_2)]^+$, the shift of the ν_{N2} band is ascribed to be electrostatic in origin. This assessment is made on the basis of the increase in positive charge of the molecule from a monocation to a dication and is supported by a shift of similar magnitude in the protonation of the CO analogue and by DFT calculations, both described below.
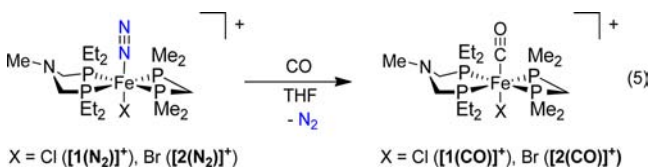
Protonation reactions of $[3(N_2)]^+$ performed at 25 °C reflect a remarkable difference in the lability of the N$_2$ ligand and stability of $[3(N_2)H]^{2+}$. Following the procedure described above, the addition of one equivalent of $[H(OEt_2)_2][B(C_6F_5)_4]$ in fluorobenzene at 25 °C resulted in the formation of $[3(N_2)H]^{2+}$ as observed by an immediate shift of the ν_{N2} band to 2139 cm^{-1}, but $[3(N_2)H]^{2+}$ is thermally unstable at 25 °C. In situ IR spectra collected at 15 s intervals reveal the intermediacy of the ν_{NN} band and the instability of $[3(N_2)H]^{2+}$, as the ν_{NN} band first shifts from 2114 to 2139 cm^{-1} and then disappears within 30 s (see Supporting Information for IR traces). In addition, ^{1}H and ^{15}N NMR spectral analysis shows that upon warming $[3(N_2)H]^{2+}$ to 25 °C, in addition to the free phosphine ligand and an unidentified diamagnetic product, ^{15}N$_2$ is ejected from the complex and H$_2$ is produced. The generation of H$_2$ and loss of N$_2$ is irreversible, and the addition of Et$_3$N to the resulting product did not regenerate $[3(N_2)]^+$.

Substitution Reactions of Ferrous N$_2$ Compounds. To examine the lability of the N$_2$ ligand in $[3(N_2)]^+$ and $[1(N_2)]^+$, ligand substitution reactions with CO were investigated. For $[3(N_2)]^+$, the displacement of N$_2$ by CO (1 atm) in fluorobenzene occurred slowly over the course of ~2 h as monitored by in situ IR spectroscopy, affording [FeH(CO)-(P^{Et}N^{Me}P^{Et})(dmpm)]$^+$ ($[3(CO)]^+$) (eq 4). The ν_{CO} band at

$$\text{[3(N}_2\text{)]}^+ \quad \xrightarrow[\text{- N}_2]{\text{CO} \atop \text{THF}} \quad \text{[3(CO)]}^+ \tag{4}$$

1938 cm^{-1} matched that of the previously reported complex.[22a] A similar rate of substitution was observed in the exchange reaction of ^{15}N$_2$ from $[3(^{15}N_2)]^+$ for ^{14}N$_2$, suggesting that N$_2$ dissociation is the rate-limiting step.

In an analogous reaction monitored by in situ IR spectroscopy, fluorobenzene solutions of $[1(N_2)]B(C_6F_5)_4$ rapidly lost N$_2$ (<15 s) upon exposure to CO (1 atm), resulting in the previously reported complex [FeCl(CO)(P^{Et}N^{Me}P^{Et})(dmpm)]$^+$ ($[1(CO)]^+$) (eq 5).[22a] Identical results were obtained for

$$\text{X = Cl ([1(N}_2\text{)]}^+\text{), Br ([2(N}_2\text{)]}^+\text{)} \quad \xrightarrow[\text{- N}_2]{\text{CO} \atop \text{THF}} \quad \text{X = Cl ([1(CO)]}^+\text{), Br ([2(CO)]}^+\text{)} \tag{5}$$

$[2(N_2)]^+$, generating [FeBr(CO)(P^{Et}N^{Me}P^{Et})(dmpm)]$^+$ ($[2-(CO)]^+$), indicating that the trans halide ligands are less effective at stabilizing the coordinated N$_2$ compared to the hydride. Halides are poor σ-donors and better π-donors than

hydride ligands, which dramatically affects the lability of the N$_2$ ligand (vide infra). The ν_{CO} bands for $[1(CO)]^+$ and $[2(CO)]^+$, 1936 and 1947 cm^{-1}, respectively, match the previously reported data.[22a,33] X-ray quality crystals of $[1-(CO)]^+$ and $[2(CO)]^+$ were grown from vapor diffusion of pentane into THF solutions, and details of the structural determinations are provided in the Supporting Information.

On the basis of ^{1}H and ^{15}N NMR spectroscopic data, the protonation reactions of $[3(N_2)]^+$ and $[2(N_2)]^+$ occur at the pendent amine. To further probe the origin and magnitude of the shift in IR frequency of the protonated species, and to validate our spectroscopic results, we examined the protonation chemistry of the CO containing complexes, $[1(CO)]^+$, $[2(CO)]^+$, and $[3(CO)]^+$.[22a] Generation of $[1(CO)]^+$ and $[2(CO)]^+$ from the addition of CO to $[1(N_2)]^+$ and $[2(N_2)]^+$ resulted in a ν_{CO} band at 1943 and 1947 cm^{-1}, respectively. The addition of one equivalent of $[H(OEt_2)_2][B(C_6F_5)_4]$ in fluorobenzene to $[1(CO)]^+$ and $[2(CO)]^+$ resulted in a shift of the ν_{CO} band by 25 (1943 to 1968) and 24 (1947 to 1971) cm^{-1}, respectively (Figure 7). The protonation of $[1(CO)]^+$
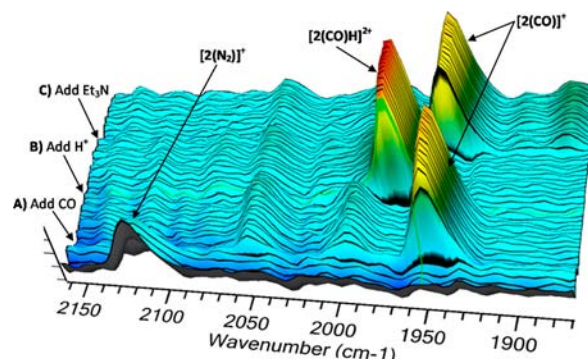

Figure 7. In situ IR plot recorded at 25 °C in fluorobenzene from the reaction of (A) $[2(N_2)]^+$ with CO to form $[2(CO)]^+$, (B) the addition of one equivalent of $[H(OEt_2)_2][B(C_6F_5)_4]$ forming $[2(CO)H]^{2+}$, and (C) the addition of one equivalent of Et$_3$N, generating $[2(CO)]^+$. Each product was stirred for 15 min before addition of the subsequent acid or base (total reaction time = 45 min).

(pK_a = 9.6 in MeCN for $[1(CO)H]^{2+}$) was previously shown to occur at the pendent amine and has been only characterized by NMR spectroscopy.[22a] The addition of 1.5 equivalent of Et$_3$N resulted in a return of the CO band back to the original position for $[1(CO)]^+$ and $[2(CO)]^+$. Treatment of $[3(CO)]^+$ with acid resulted in a 22 cm^{-1} shift, and $[3(CO)]^+$ could be regenerated by adding an equivalent of Et$_3$N to $[3(CO)H]^{2+}$ (see Supporting Information). The protonation of $[3(CO)]^+$ (pK_a = 10.5 in MeCN for $[3(CO)H]^{2+}$) was also previously shown to occur at the pendent amine and was only characterized by NMR spectroscopy.[22a]

The formation of both dihydrogen and ammonia by nitrogenase enzymes prompted us to explore the displacement of dinitrogen by dihydrogen and ammonia. Exposure of a degassed THF-d_8 solution of $[3(N_2)]B(C_6F_5)_4$ to one atmosphere of H$_2$ resulted in complete conversion to trans-[FeH(H$_2$)(P^{Et}N^{Me}P^{Et})(dmpm)]$^+$ ($[3(H_2)]^+$),[22a] over the course of 48 h as monitored by ^{31}P NMR, with multiplets at δ 49.9 and 3.4 and a very broad peak at δ −8.7 in the ^{1}H NMR spectrum (eq 6). Removal of the dihydrogen atmosphere and introduction of an atmosphere of ^{15}N$_2$ resulted in complete conversion back to $[3(^{15}N_2)]B(C_6F_5)_4$ over the course of 3 h,
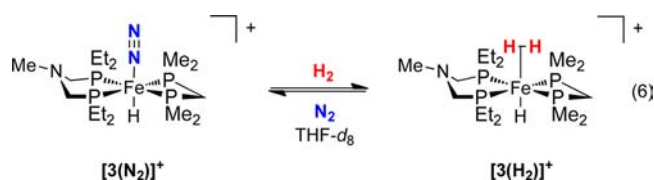
indicating that the binding of both N_2 and H_2 is reversible. The increased rate of binding dinitrogen suggests a higher lability of the dihydrogen adduct and that $[FeH(P^{Et}N^{Me}P^{Et})(dmpm)]^+$ has a slight preference for dinitrogen binding.

Treatment of a pale yellow, degassed THF-d_8 solution of $[3(N_2)]B(C_6F_5)_4$ with one atmosphere of $^{15}NH_3$ resulted in a change to dark yellow after 30 min at 25 °C (eq 7). Complete
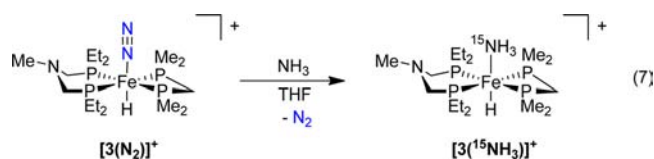
conversion to $[FeH(^{15}NH_3)(P^{Et}N^{Me}P^{Et})(dmpm)]^+$ ($[3-(^{15}NH_3)]^+$) required about 5 h as determined by ^{31}P and ^1H NMR spectroscopy. Prolonged exposure (beyond 12 h) to an excess of NH_3 resulted in dissociation of the phosphine ligands from the Fe center. ^{31}P NMR resonances shifted from δ 38.8 and -0.8 for $[3(N_2)]B(C_6F_5)_4$ to 47.9 and 2.6 for $[3(^{15}NH_3)]$-$B(C_6F_5)_4$, and a sharp resonance in the ^{15}N NMR spectrum at -433.1 confirmed the presence of a bound $^{15}NH_3$ ligand. Additionally, a concomitant shift of the hydride resonance in the ^1H NMR spectrum from δ -14.5 to -25.5 indicated ligand exchange had occurred. Protons of the bound amine ligand were anticipated to resonate in the upfield region around δ -0.1. For example, in previously reported Fe-NH_3 complexes of this type, the NH_3 protons were assigned as a broad singlet at δ -1.61 and -0.09 for trans-$[Fe(H)(NH_3)(dmpe)_2]$-$[C_{13}H_9][34]$ and $[Fe(H)(NH_3)(dmpe)_2][BPh_4][35]$ (both in THF-d_8), respectively, and -0.86 for trans-$[Fe(H)(NH_3)((P-(C_3H_6OMe)_2CH_2)_2)_2][BPh_4]$ in $C_6D_6[36]$ However, for $[3-(^{15}NH_3)]B(C_6F_5)_4$, no resonances were found in this region of the ^1H NMR spectrum. Further analysis of the sample by a ^1H-^{15}N HSQC correlation experiment located the ^1H resonance of the bound amine ligand at δ 1.61, correlating to the ^{15}N signal at δ -433.1. A similar downfield resonance for the amine protons was also observed for $[3(^{15}NH_3)]BPh_4$, which eliminated a hydrogen bonding interaction with the fluorine atoms in the anion (see description of solid state structure below) as the cause of the unusually downfield resonance for the amine protons. It is unclear if an interaction with a pendent amine group in the $P^{Et}N^{Me}P^{Et}$ ligand is responsible for this observation.

In contrast to the rapid ligand exchange for $[3(^{15}NH_3)]B-(C_6F_5)_4$, Tyler and co-workers reported that the treatment of a THF solution of trans-$[FeH(N_2)((P(C_3H_6OMe)_2CH_2)_2)_2]^+$ with a saturated NH_3 solution required two days to obtain full conversion to trans-$[FeH(NH_3)((P(C_3H_6OMe)_2CH_2)_2)_2]^+$ and that an argon atmosphere is required for this reaction to occur.[36] Investigating the ligand exchange reaction in the opposite direction, exposure of a THF-d_8 solution of isolated $[3(^{15}NH_3)]B(C_6F_5)_4$ to 1 atm of $^{15}N_2$ resulted in a mixture of $[3(^{15}NH_3)]B(C_6F_5)_4$ and $[3(N_2)]B(C_6F_5)_4$ with an equilibrium constant at 25 °C of ~2.5.

Crystallization of $[3(^{15}NH_3)]B(C_6F_5)_4$ by the vapor diffusion of pentane into fluorobenzene under an argon atmosphere resulted in X-ray quality crystals. Crystallographic analysis of $[3(^{15}NH_3)]B(C_6F_5)_4$ confirmed the presence of the Fe bound NH_3 ligand, with an Fe-NH_3 bond distance of 2.111(3) Å (Figure 8). The observed Fe-NH_3 bond distance in
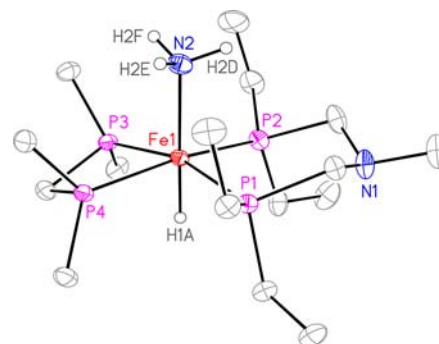

Figure 8. Molecular structure of the cation $[FeH(^{15}NH_3)(P^{Et}N^{Me}P^{Et})$-$(dmpm)]^+$ ($[3(^{15}NH_3)]^+$). Thermal ellipsoids are drawn at 30% probability. The hydrogen atoms (except for the Fe-H and NH_3) and $B(C_6F_5)_4^-$ anion are omitted for clarity. Selected bond distances (Å) and angles (deg): P(1)-Fe(1) = 2.209(1), P(2)-Fe(1) = 2.195(1), P(3)-Fe(1) = 2.210(1), P(4)-Fe(1) = 2.207 (1), Fe(1)-N(2) = 2.111(3), Fe(1)-H(1A) = 1.42(3), P(2)-Fe(1)-P(1) = 90.87(4), P(3)-Fe(1)-P(4) = 73.69(1), N(2)-Fe(1)-H(1A) = 178.9(13).

$[3(^{15}NH_3)]^+$ is in accord with the Fe-NH_3 distance reported for $[FeH(NH_3)(dmpe)_2]OH$ (2.103 Å)[34] and is within the range of other previously reported Fe-NH_3 complexes (2.008-2.190 Å).[37] In addition, the six-membered ring of the $P^{Et}N^{Me}P^{Et}$ ligand is in the chair configuration with the pendent amine positioned exo with respect to the NH_3. Thus, in the solid state there does not appear to be an interaction between the pendent methylamine group and the protons of the Fe bound NH_3. However, in the crystal lattice a hydrogen bonding interaction (~3.2 Å) was observed between the fluorine substituents of the $B(C_6F_5)_4$ anion and the protons of the Fe bound NH_3 group (see Supporting Information). The remaining bond lengths and angles of $[3(^{15}NH_3)]B(C_6F_5)_4$ were found to be similar to those of $[3(N_2)]B(C_6F_5)_4$ (see above).

Electrochemistry of Ferrous-N_2 Complexes. The electrochemistry of $[3(N_2)]BPh_4$ was investigated and compared to $[FeH(N_2)(dmpe)_2]BPh_4$,[23] to further understand the effect of pendent amines on the proton transfer chemistry of the N_2 reduction. $[FeH(N_2)(dmpe)_2]BPh_4$ has been previously shown to produce NH_3 in 4% yield when treated with H_2SO_4.[11a] The cyclic voltammogram of $[FeH(N_2)-(dmpe)_2]BPh_4$ exhibits an irreversible reduction wave assigned as the $Fe^{II/I}$ couple at -1.89 V in CH_2Cl_2. All reduction potentials are referenced to $Cp_2Fe^{0/+}$ at 0 V using $Cp^*_2Fe^{0/+}$ ($E_{1/2} = -0.53$ V) as a reference. An irreversible peak corresponding to the oxidation of the iron hydride is observed at -0.60 V in CH_2Cl_2. For comparison, the irreversible $Fe^{II/I}$ reduction wave of $[3(N_2)]BPh_4$ at -24 °C (-2.58 V) was observed at a 0.25 V more negative potential than that of $[FeH(N_2)(dmpe)_2]BPh_4$ (see the Supporting Information for the voltammogram).

To study the effect of the added acid on the $Fe^{II/I}$ redox couple, cyclic voltammetry of $[FeH(N_2)(dmpe)_2]BPh_4$ and $[3(N_2)]BPh_4$ was performed in the presence of acid. The

addition of one equivalent of $[H(OEt_2)_2][B(C_6F_5)_4]$ to methylene chloride solutions of $[FeH(N_2)(dmpe)_2]BPh_4$ resulted in a proton reduction wave that is attributed to the direct reduction of H^+ to H_2 by the electrode (Figure 9), with
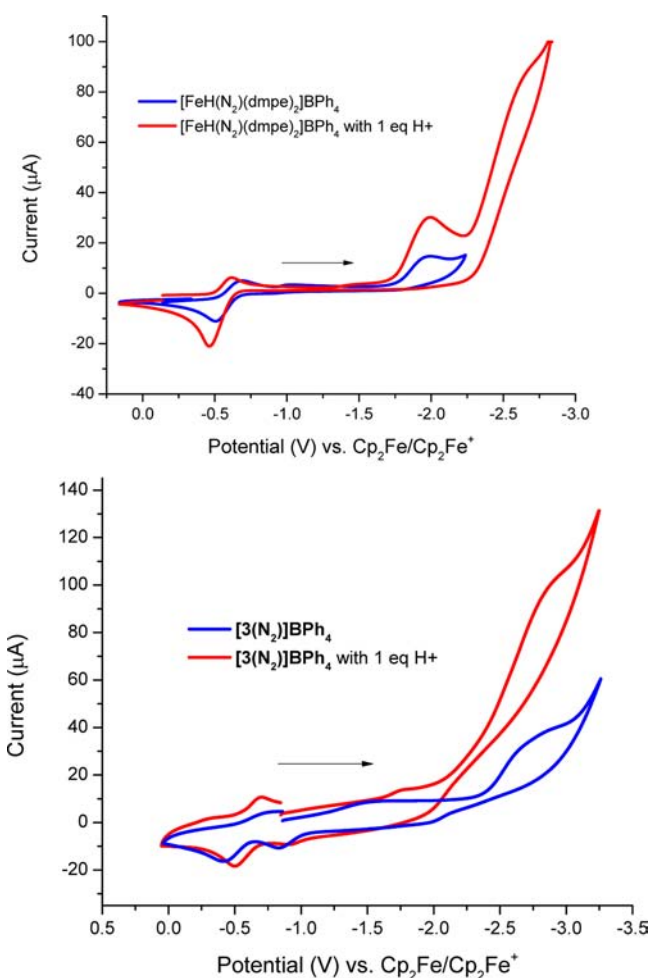

Figure 9. Cyclic voltammograms showing the effect of acid on (top) $[FeH(N_2)(dmpe)_2]BPh_4$ (25 °C) and (bottom) $[3(N_2)]BPh_4$ (−24 °C), in CH_2Cl_2. Acid = $[H(OEt_2)_2][B(C_6F_5)_4]$. Electrolyte = 0.1 M $[Bu_4N][B(C_6F_5)_4]$; scan rate = 100 mV/s.

an onset of the proton reduction occurring at a potential of −2.26 V. As indicated above, when one equivalent of acid is added to $[3(N_2)]BPh_4$, the protonation occurs on the pendent amine as opposed to the N_2 ligand, and through cyclic voltammetry experiments we aimed to probe the effect of this protonation on the reduction potential of the $Fe^{II/I}$ couple. The protonation reaction was undertaken at −24 °C because $[3(N_2)H]^{2+}$ is more stable at lower temperatures. The addition of one equivalent of $[H(OEt_2)_2][B(C_6F_5)_4]$ to $[3(N_2)]BPh_4$ resulted in a shift of the onset potential of the reduction wave corresponding to the $Fe^{II/I}$ couple to shift about 0.33 V to more positive potentials (Figure 9). To compare the effect of protonation of the pendent amine on the redox potential of the iron center, we also examined the redox chemistry of $[3(CO)]^+$. Unlike the IR studies described above that resulted in almost identical vibrational frequency shifts upon protonation of the pendent amine for both $[3(N_2)]^+$ and $[3(CO)]^+$, the redox potential for the $Fe^{II/I}$ couple was found to differ by 0.10 V, where the protonation of $[3(N_2)]^+$ exhibits a larger shift
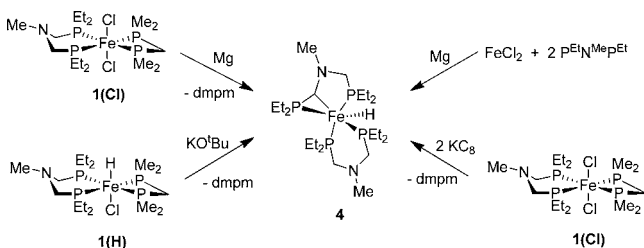
in redox potential. Similar results were observed by Sellmann and Sutter where protonation or alkylation of the thiolate of $[Fe(CO)(SC_6H_4SC_2H_4NHC_2H_4SC_6H_4S)]$ was found to shift the redox potential by 0.50−0.70 V per protonation or alkylation.[5c] The larger shift in redox potential observed in Sellmann and Sutter's complexes is attributed to the closer proximity of the proton/alkyl group to the iron center.

Protonation Reactions to Form NH_3. Reports of ammonia production by protonation of ferrous-N_2 complexes are rare, and yields of ammonia are low (<4%, with respect to the metal, in the case of the reaction of trans-$[FeH(N_2)(dmpe)_2]^+$ with H_2SO_4).[11a] Rather than stoichiometric reduction of N_2 to ammonia, more common observations include liberation of N_2 and H_2, or no reaction.[38] Higher yields (up to 82% with respect to the metal) of ammonia upon protonolysis with strong acids such as HCl, H_2SO_4, or triflic acid have been reported for low-valent Fe^0 dinitrogen complexes supported by a variety of chelating diphosphine ligands such as $Fe(N_2)(dmpe)_2$,[2] where the electrons are supplied by the low valent iron center.

To probe whether the ferrous-N_2 complexes supported by diphosphine ligands containing a pendent amine could generate NH_3, we examined the reaction of $[3(N_2)]^+$ with excess strong acid. A 0.01 M $[3(N_2)]BPh_4$ in THF solution was treated with 50 equivalents of concentrated H_2SO_4, resulting in a lighter yellow colored solution and the formation of a white solid. After 3 h, a ^1H NMR spectrum of the reaction products in DMSO-d_6 showed no ammonium (7.0 ppm).[13] It was reported that $[FeH(N_2)(dmpe)_2]BPh_4$ gave 4% ammonia under similar conditions,[11a] but in our hands, treatment of $[FeH(N_2)(dmpe)_2]BPh_4$ with 50 equivalents of H_2SO_4 as described above yielded only protonated dmpe; NH_4^+ was not detected by NMR spectroscopy. A similar result was observed by Henderson, where only a protonated ligand was observed following the addition of HCl to $[FeH(N_2)(depe)_2]BPh_4$.[38a]

Attempts to Synthesize Fe(0)-N_2 Complexes. Due to the absence of reactivity toward H^+ at the N_2 ligand in the Fe^{II} complexes, we examined the reduction of these complexes, with the targets being the Fe^0-N_2 complexes $Fe(N_2)(dmpm)(P^{Et}N^{Me}P^{Et})$ or $Fe(N_2)(P^{Et}N^{Me}P^{Et})_2$. Reduction of green solutions of $1(Cl)$ or $2(Br)$ with Mg or KC_8 resulted in the formation of an orange product. ^{31}P NMR spectra (THF-d_8) of the reaction mixture showed the presence of free dmpm and four multiplets at δ 14.9, 40.6, 53.2, and 72.6, consistent with four inequivalent phosphorus atoms. The ^1H NMR spectrum contains a multiplet at δ −13.86, indicating the presence of a hydride ligand bound to the Fe center, and a medium intensity ν_{FeH} band was observed at 1900 cm^{-1} (KBr) in the IR spectrum. Dehydrohalogenation reactions by the addition of one or more equivalents of KO^{t}Bu to $1(H)$ and $2(H)$ resulted in the formation of the same Fe−H product. Due to the expected trigonal bipyramidal coordination geometry of the five-coordinate Fe^0-N_2 complex, it is not surprising that dmpm (bite angle ~73° in $1(Cl)$) dissociates from the metal center upon the change in geometry. The reduction of $FeBr_2$ with Mg in the presence of two equivalents of $P^{Et}N^{Me}P^{Et}$ (bite angle ~92° in in $1(Cl)$) was attempted as a synthetic route to $Fe(N_2)(P^{Et}N^{Me}P^{Et})_2$. However, instead of detecting the expected intense ν_{NN} band of this orange product in the IR spectrum, the same ν_{FeH} band was observed at 1900 cm^{-1}, and ^{31}P and ^1H NMR spectra matched the spectroscopic data of the reduction and dehydrohalogenation product of $2(Cl)$ and $2(H)$, respectively (Scheme 2). The presence of the Fe−H in

Scheme 2. Reactions That Form Complex HFe(Et$_2$PC(H)N(Me)CH$_2$PEt$_2$)(P^{Et}N^{Me}P^{Et}) (4)

reversible, and attempts to avoid C—H activation of the methylene group of the P^{Et}N^{Me}P^{Et} ligand by performing the reduction of FeBr$_2$ with Mg and two equivalents of P^{Et}N^{Me}P^{Et} under elevated N$_2$ pressures (up to 40 atm) were unsuccessful, resulting in the production of **4**.

Computational Analysis. Computational analysis employing density functional theory (DFT) based electronic structure methods was used to provide insight into N$_2$ binding, acid reactivity, and redox potentials of the Fe complexes. We first examined the binding affinity of N$_2$ in [3(N$_2$)]$^+$ and [1(N$_2$)]$^+$ as well as the protonated species [3(N$_2$)H′]$^{2+}$ and [1(N$_2$)H′]$^{2+}$ (Figure 11). The calculated free energy binding affinity of N$_2$ in

the product suggests oxidative addition of the C—H bond of the P^{Et}N^{Me}P^{Et} ligand to Fe occurred as did ligand redistribution in the FeX$_2$(P^{Et}N^{Me}P^{Et})(dmpm) and FeHX(P^{Et}N^{Me}P^{Et})(dmpm) reactions which contain free dmpm. The reaction could be envisioned to occur by deprotonation at the methylene position followed by metal coordination, or by deprotonation of the hydride, followed by oxidative addition of the C—H bond.

Crystallographic analysis of the orange product described above confirmed the molecular structure, as shown in Figure 10. Oxidative addition of the C—H of a methylene group in the
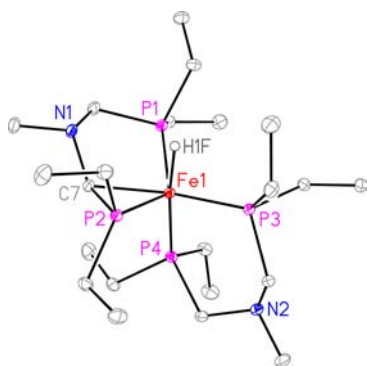

Figure 10. Molecular structure of complex HFe(Et$_2$PC(H)N(Me)-CH$_2$PEt$_2$)(P^{Et}N^{Me}P^{Et}), **4**. Thermal ellipsoids are shown at 30% probability. Selected bond distances (Å) and angles (deg): P(1)—Fe(1) = 2.152(1), P(2)—Fe(1) = 2.183(1), P(3)—Fe(1) = 2.149(1), P(4)—Fe(1) = 2.171(1), Fe(1)—C(7) = 2.068(1), Fe(1)—H(1F) = 1.479(18), C(7)—Fe(1)—P(2) = 49.69(4), C(7)—Fe(1)—P(1) = 83.09(4), P(2)—Fe(1)—P(1) = 124.68(18), P(3)—Fe(1)—P(4) = 91.41(12).

P^{Et}N^{Me}P^{Et} ligand backbone produced the neutral iron hydride complex HFe(Et$_2$PC(H)N(Me)CH$_2$PEt$_2$)(P^{Et}N^{Me}P^{Et}) (**4**). Coordination of the methylene carbon to the iron center forms a three-membered ring, where the methylene carbon bound to the Fe center is trans to a phosphorus atom from the other P^{Et}N^{Me}P^{Et} ligand. The unmodified P^{Et}N^{Me}P^{Et} ligand in this complex has a bite angle of 91.41(12)°. Similar C—H activation of the methylene group in a phosphine based ancillary ligand was identified by Karsch and co-workers, in which an Fe^0 complex containing two (Me$_2$PCH$_2$)$_2$PMe ligands undergoes intramolecular oxidative addition, forming a hydrido—Fe^{II} complex.[39] Furthermore, in a related example describing the preparation of an Fe^0—N$_2$ complex, reduction of FeCl$_2$(depe)$_2$ with sodium-naphthalene under an argon atmosphere formed Fe(depe)$_2$, which undergoes oxidative addition of a C—H bond of the ethyl group to form the hydrido—Fe^{II} complex. This process was reversible, as this product was readily converted to Fe(N$_2$)(depe)$_2$ when placed under N$_2$.[40] In the present case, the C—H activation was not

Figure 11. Possible products from protonation of [3(N$_2$)]$^+$ and [1(N$_2$)]$^+$.

Table 1. Binding Affinity of N$_2$ and CO to Iron Complexes Containing a Protonated and Non-Protonated Pendent Amine

	binding affinity of ligand to Fe complexes (kcal/mol)			
ligand	[3(N$_2$)]$^+$/ [3(CO)]$^+$	[1(N$_2$)]$^+$/ [1(CO)]$^+$	[3(N$_2$)H′]$^{2+}$/ [3(CO)H′]$^{2+}$	[1(N$_2$)H′]$^{2+}$/ [1(CO)H′]$^{2+}$
N$_2$	10.1	7.4	8.4	6.4
CO	36.0	33.2	33.9	32.1

[3(N$_2$)]$^+$ and [1(N$_2$)]$^+$ is 7.4 and 10.1 kcal/mol (Table 1), respectively. The small N$_2$ binding affinity indicates that N$_2$ is weakly coordinated. For comparison, the binding affinity of CO for the corresponding species, [3(CO)]$^+$, [1(CO)]$^+$, [3(CO)-H′]$^{2+}$, and [1(CO)H′]$^{2+}$ was also determined (Table 1). Compared to N$_2$, the binding affinity of CO in [3(CO)]$^+$ and [1(CO)]$^+$ is 36.0 and 33.2 kcal/mol (Table 1) respectively, which is more favorable by 26 kcal/mol than N$_2$ binding. The much larger binding affinity of CO vs N$_2$ and a larger binding affinity of N$_2$ in [3(N$_2$)]$^+$ than in [1(N$_2$)]$^+$ verify the experimental observations that CO was found to displace N$_2$ from [3(N$_2$)]$^+$ and [1(N$_2$)]$^+$ but with a slower exchange rate in [3(N$_2$)]$^+$ than in [1(N$_2$)]$^+$.
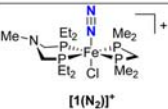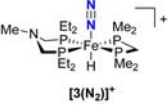
To address the relative binding/ligand strengths of N$_2$ and CO, we follow a similar methodology as our previous work on Cr—N$_2$ complexes, where an NBO based fragment analysis is employed.[21b] This approach avoids well-known pitfalls of population analysis performed with large basis sets and

additionally affords energy values for the various orbital interactions to provide a quantitative description of the bonding.[41] The $Fe^{II}(d)-N_2(\sigma)$ interaction is found to be about 150 kcal/mol for complexes $[3(N_2)]^+$ and $[1(N_2)]^+$, whereas the $Fe^{II}(d)-N_2(\pi^*)$ interaction is found to be appreciably smaller, ca. 10–12 kcal/mol. Thus, N_2 can be viewed as mainly a σ-donor but exhibits negligible π-acceptor capability for these Fe^{II} species. In comparison, CO is found to be a stronger σ-donor ($Fe^{II}(d)-CO(\sigma)$ interaction energy about 220 kcal/mol) and a stronger π^* acceptor ($Fe^{II}(d)-CO(\pi^*)$ interaction energy about 32 kcal/mol). A similar analysis on hypothetical Fe^0 complexes $Fe(L)(P^{Et}N^{Me}P^{Et})$-(dmpm) (L = N_2, CO) further confirms our bonding assessment. In the Fe^0 complexes, the σ-bonding interaction energy decreases to 99 and 215 kcal/mol for N_2 and CO, respectively, in accord with the expectation that Fe^0 will be a weaker acceptor than Fe^{II}. Likewise, the $Fe^0(d)-L(\pi^*)$ interaction energy increased to 37 and 63 kcal/mol for N_2 and CO, in ac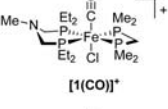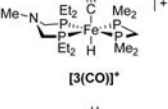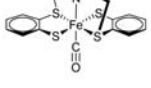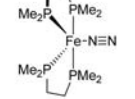cord with the expectation that Fe^0 will be a stronger π-donor. This description of binding is in qualitative accord with the preference for CO to bind to the Fe complexes described above, suggesting CO is also a poor π-acceptor for Fe^{II} species and an appreciably stronger π-acceptor on Fe^0. In contrast, N_2 has negligible π-acceptor strength on Fe^{II} and acts as only a moderate π-acceptor on Fe^0.

In accord with this bonding picture, there is negligible charge transfer ($\ll 0.1e^-$) from the metal to the N_2 in $[3(N_2)]^+$. Thus, to explain the blue shift of the IR frequency and observed lengthening on the N–N bond, we resort to a qualitative picture where these observations are attributed to the mixing of π/π^* states of N_2 upon binding to an electron-rich metal center. As in our work on $Cr-N_2$ complexes,[21b] it was found that a simple electrostatic model where a negative charge on the metal/phosphine core polarizes the bound N_2 results in a lowering of N–N bond order (see Supporting Information for an analysis of N–N bond order, bond length increase, and IR frequency shift from an electrostatic model). Interpretation of our results on N_2 and CO binding in this context is more appropriate to explain our observations than the more traditional approach based on metal-π^* back-bonding, which, as outlined above, has negligible energetic contribution in the Fe^{II} species.

For the protonated species, $[3(N_2)H']^{2+}$ and $[1(N_2)H']^{2+}$, where the protons reside on the pendent amine, the calculated binding affinity of N_2 was found to be ~1–2 kcal/mol lower than in nonprotonated complexes. Similar results were found for the corresponding CO analogues, $[3(CO)H']^{2+}$ and $[1(CO)H']^{2+}$. Harmonic vibrational analysis showed that when protons were added to complexes $[3(N_2)]^+$ and $[1(N_2)]^+$ and complexes $[3(CO)]^+$ and $[1(CO)]^+$, the ν_{NN} and ν_{CO} bands increased by 20 and 22 and by 23 and 25 cm^{-1}, respectively (Table 2). As a comparison to the IR shifts of related N_2 and CO containing Fe complexes, protonation of the thiolate sulfur in $[Fe(CO)(SC_6H_4SC_2H_4NHC_2H_4SC_6H_4S)]$ or to either the Fe center or N_2 ligand in $Fe(N_2)(dmpe)_2$ resulted in a more dramatic increase in IR shifts of 39[5c] and 120 and a decrease in IR shift of 395 cm^{-1},[30] respectively, Table 2. Further analysis of N_2 and CO ligands in $[3(N_2)]^+$ and $[3(CO)]^+$ by evaluating the Wiberg bond index (WBI), obtained from a NBO analysis, indicated the N–N bond order increased from 2.70 to 2.74 upon protonation while the WBI of Fe–N decreased from 0.48 to 0.44 upon protonation. Similar trends are observed for the CO analogues, where the

Table 2. Comparison of Experimental and Computational IR Shifts for Protonation of Complexes $[1(N_2)]^+$, $[3(N_2)]^+$, $[1(CO)]^+$, and $[3(CO)]^+$

Complex	Experimental IR Shift ($\nu_{N\equiv N}$ or $\nu_{C\equiv O}$) from H$^+$ Addition (cm^{-1})	Computational IR Shift ($\nu_{N\equiv N}$ or $\nu_{C\equiv O}$) from H$^+$ Addition (cm^{-1})
$[1(N_2)]^+$	23	20
$[3(N_2)]^+$	25	22
$[1(CO)]^+$	24	23
$[3(CO)]^+$	22	25
(Fe thiolate complex)	39[a]	
(Fe(N$_2$)(dmpe)$_2$)		120[b]
		-395[c]

[a]This IR shift corresponds to alkylation of a sulfur atom with Et$^+$.[5c]
[b]This corresponds to the IR shift of protonation of the metal center.[30]
[c]This corresponds to the IR shift of protonation of the N_2 ligand.[30]

WBI of the C–O increased from 2.05 to 2.10 while the WBI of the Fe–C decreased from 0.74 to 0.70 upon protonation. The small change in bond order is consistent with the small shift in the IR bands and the small decrease in binding affinity of N_2 and CO. Further electron density analysis (Figure 12) shows that the *change* in electron density upon protonation mainly occurred at the local region where the proton resides (pendent
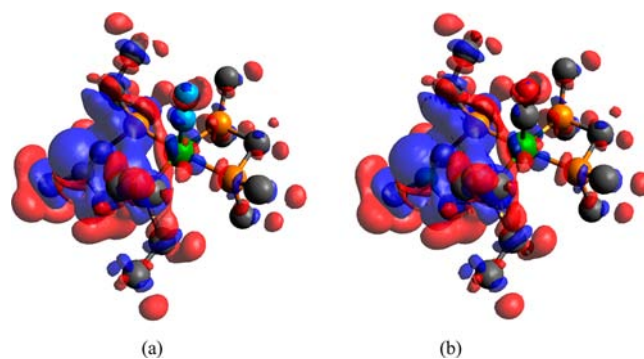
Figure 12. The electron density difference (isovalue = 0.0012) between the nonprotonated species and with a proton at the pendent amine. (a) $[3(N_2)]^+$ and (b) $[3(CO)]^+$. Depletion of electron density is represented by red, while increased electron density is represented by blue. Methyl and methylene protons are removed for clarity. Phosphorus = orange, nitrogen = light blue, carbon = gray, hydrogen = white, iron = green, and oxygen = red.

amine). There is a small change in electron density of the N_2 and CO ligands, where the electron density decreased slightly at distal N and O while it slightly increased at the proximal N and C. From these observations, coupled with our above analysis of the Fe−N_2 and Fe−CO bonding, the interaction of N_2 with Fe can be understood as an electrostatic effect, where protonation at the pendent amine depolarizes the N_2 ligand and thus strengthens the N−N π bond and weakens the overall interaction between the N_2 and Fe center.

Modulating the basicity of the iron-bound N_2 ligand and the pendent amine in complexes similar to $[3(N_2)]^+$ is important in controlling the reactivity toward protons. Therefore, a quantitative assessment of the preferred protonation sites in $[3(N_2)]^+$ is valuable for interpreting the reactivity and spectroscopic data. To quantify the basicity of the N_2 ligand in the ferrous iron complexes and to determine the conditions required for proton transfer to the N_2 ligand from the pendent amine, we calculated the proton affinity of nitrogen on the pendent amine and the distal nitrogen atom of coordinated N_2. The proton affinity of the pendent amine of $[3(N_2)]^+$ was calculated to be 43.5 kcal/mol higher than that of the N_2 ligand (31.9 pK_a units more basic for $[3(N_2)H']^{2+}$ versus $[3(N_2)-H'']^{2+}$). In the case of $[1(N_2)]^+$, the proton affinity of the pendent amine is lower than that of $[3(N_2)]^+$ (0.9 kcal/mol or 0.7 pK_a units more acidic for $[1(N_2)H']^{2+}$ versus $[3(N_2)-H']^{2+}$), and the pendent amine was calculated to be 52.8 kcal/mol higher (or 38.7 pK_a units more basic for $[1(N_2)H']^{2+}$ versus $[3(N_2)H'']^{2+}$) than the N_2 ligand. Therefore, it is not surprising that the pendent amine was protonated when protons were added to these complexes. Replacement of the trans chloride ligand by hydride increases the proton affinity (basicity) of pendent amine and N_2 ligands. This indicates that the introduction of a better electron donating ligand results in an increase of the electron density at the metal center, which in terms of our picture of Fe−N_2 bonding based on an inductive effect would increase the polarization of the bound N_2 and render it more basic.

To further examine the effect of the trans ligand on the basicity of the N_2 ligand upon protonation, the frontier molecular orbitals of $[3(N_2)]^+$ and $[1(N_2)]^+$ were determined and compared to the frontier molecular orbitals of $[3(N_2)H']^{2+}$ and $[1(N_2)H']^{2+}$. It was found that the HOMO resided on the pendent amine for $[3(N_2)]^+$ and $[1(N_2)]^+$ (Figure 13 and Supporting Information). Upon protonation of $[3(N_2)]^+$ and $[1(N_2)]^+$ at the pendent amine, resulting in complexes $[3(N_2)H']^{2+}$ and $[1(N_2)H']^{2+}$, respectively, the HOMOs
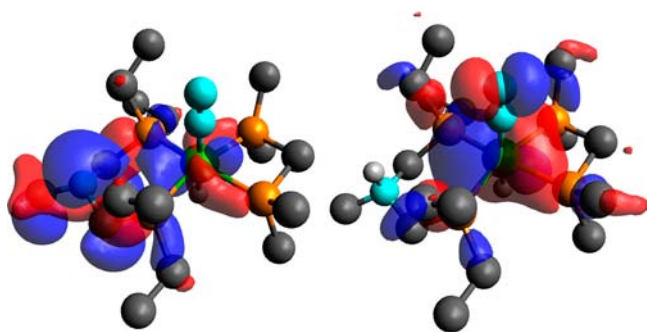

Figure 13. Comparison of the HOMOs of (left) $[3(N_2)]^+$ and (right) $[3(N_2)H']^{2+}$. Methyl and methylene protons are removed for clarity. Phosphorus = orange, nitrogen = light blue, carbon = gray, hydrogen = white, iron = green.

move from the pendent amine to the iron center/N_2 ligand and to the chloride ligand, respectively (Figure 13). The larger degree of electron density present on the N_2 ligand upon protonation of $[3(N_2)]^+$ is attributed to the increased basicity of the N_2 ligand of $[3(N_2)H']^+$ vs $[1(N_2)H']^+$ (see below and Supporting Information). This also indicates that by increasing the electron density at the metal center by changing the ligand trans to dinitrogen that the electron density can be increased at the N_2 ligand, to encourage proton transfer from the pendent amine to the dinitrogen ligand.

The high acidities of the protonated N_2 ligands of $[3(N_2)H'']^{2+}$ and $[1(N_2)H'']^{2+}$ indicate that PCET will be required to promote the reduction of N_2 to NH_3. To probe the effect of PCET on $[3(N_2)]^+$, we calculated the redox potential for the $Fe^{II/I}$ couple of $[3(N_2)]^+$ and $[3(N_2)H']^{2+}$. The calculated $Fe^{II/I}$ redox potential of $[3(N_2)H']^{2+}$ shifts to a more positive value by 0.44 V, which is comparable to the experimental value of 0.33 V. For comparison, we also calculated the redox potential for the $Fe^{II/I}$ couple of $[3(CO)]^+$ and $[3(CO)H']^{2+}$. The calculated $Fe^{II/I}$ redox potential of $[3(CO)H']^{2+}$ shifts to a more positive value 0.11 V less than observed with $[3(N_2)H']^{2+}$, which is almost identical to the values measured experimentally.

To promote proton transfer to the N_2 ligand from the pendent amine, the low valent complex, $Fe^0(N_2)(P^{Et}N^{Me}P^{Et})$-(dmpm), was probed computationally. The pK_a of $[Fe^0(N_2)-(P^{Et}N^{Me}HP^{Et})(dmpm)]^+$ increased by 11 pK_a units vs $[3(N_2)-H']^{2+}$, while the pK_a of $[Fe^0(HN_2)(P^{Et}N^{Me}P^{Et})(dmpm)]^+$ dramatically increased by about 43 pK_a units. The reduction of Fe^{II} to Fe^0 increases the basicity of the N_2 ligand to the same level as that of pendent amine, which would allow a facile proton transfer to the N_2 ligand from the pendent amine. However, as described above, reduction of **1(Cl)** or dehydrohalogenation of **1(H)** led to C−H activation of the methylene group of the $P^{Et}N^{Me}P^{Et}$ ligand resulting in complex **4**. Computationally, oxidative addition of the methylene group was found to be 4 kcal/mol more favorable than N_2 binding to $Fe(P^{Et}N^{Me}P^{Et})_2$, thus explaining the experimental results where C−H activation was observed at elevated N_2 pressure.

■ CONCLUSIONS

Ferrous dinitrogen complexes supported by the diphosphine ligand $P^{Et}N^{Me}P^{Et}$ containing a pendent amine base have been synthesized and characterized. These complexes undergo reactions with acid, resulting in the protonation of the pendent amine with subsequent loss of N_2 rather than protonation at the N_2 ligand. Protonation of these ferrous-dinitrogen complexes at low temperature results in stabilization of the protonated complexes, and the addition of base deprotonates the pendent amine, regenerating the starting $Fe^{II}(N_2)$ complex. Similar results were observed for the related carbonyl complexes, except that the protonated complexes were stable at 25 °C. Although the incorporation of pendent amines in ferrous-dinitrogen complexes does not lead to proton transfer to the N_2 ligand, protonation of the pendent amine shifts the reduction potential of the $Fe^{II/I}$ couple to more positive potentials. Protonation of the pendent amine resulted in strengthening of the N−N bond (higher $\nu_{N≡N}$ by 25 cm^{-1}) of the dinitrogen ligand. This finding has implications in regards to the nature of the recently proposed N_2 binding site of nitrogenases,[7e] as protonation of a pendent base results in a decrease of the N_2 binding affinity. Thus, the electrostatic effects of nearby protons and the role of PCET in the

stabilization of N_2 binding and reduction to NH_3 is worthy of consideration in the mechanistic discussion of nitrogenase and in the design of molecular catalysts for N_2 reduction. Chemical reduction of the reported ferrous complexes resulted in oxidative addition of the C—H bond of the methylene carbon of the $P^{Et}N^{Me}P^{Et}$ ligand as opposed to forming an $Fe^0—N_2$ complex. These experimental results were validated computationally, and it was shown that ferrous-dinitrogen complexes are incapable of aiding in the protonation of coordinated N_2, as the pK_a determination of protonation at the coordinated N_2 was found to be highly unfavorable; less basic pendent amines are needed. Computational results also show that incorporation of a strong electron donating ligand trans to the dinitrogen ligand or a more electron-rich metal can be used to tune the basicity of the dinitrogen ligand. Further investigation of the tuning of pendent amines to facilitate proton transfer to low-valent dinitrogen complexes is currently under intense investigation in our laboratory.

■ EXPERIMENTAL SECTION

Synthesis and Materials. All synthetic procedures were performed under an atmosphere of N_2 using standard Schlenk or glovebox techniques. Unless described otherwise, all reagents were purchased from commercial sources and were used as received. Solvents were dried by passage through activated alumina in an Innovative Technology, Inc., PureSolv solvent purification system. Deuterated NMR solvents THF-d_8, toluene-d_8, and benzene-d_6 were purchased from Cambridge Isotope Laboratories, dried over NaK, and vacuum transferred before use. $K[B(C_6F_5)_4]$ was purchased from Boulder Scientific. Ferrous chloride, ferrous bromide, and 1,2-bis(dimethylphosphino)methane were purchased from Strem Chemicals, Inc. and used as received. Magnesium powder, paraformaldehyde (95%), methylamine in ethanol (33 wt %), and HCl (2 M in ether) were purchased from Sigma-Aldrich. $FeCl_2(P^{Et}N^{Me}P^{Et})(dmpm)$,[22a] $FeHCl(P^{Et}N^{Me}P^{Et})(dmpm)$,[22a] $P^{Et}N^{Me}P^{Et}$,[42] and $[NBu_4][B(C_6F_5)_4]$[43] were synthesized according to literature preparations. $[H(OEt_2)_2][B-(C_6F_5)_4]$ was prepared according to a modified literature procedure,[44] see below. NMR spectra were recorded on a Varian Inova or NMR S 500 MHz spectrometer. ^1H chemical shifts are referenced to residual protio impurity in deuterated solvent. ^{31}P chemical shifts are proton decoupled unless otherwise noted and referenced to H_3PO_4 as an external reference. ^{15}N NMR chemical shifts are externally referenced to $CH_3^{15}NO_2$ ($\delta = 0$). Infrared spectra were recorded on a Thermo Scientific Nicolet iS10 FT-IR spectrometer at ambient temperature and under a purge stream of nitrogen gas. Solid-state FT-IR samples were prepared as KBr pellets. Elemental analysis was performed by Atlantic Microlabs, Norcross, GA. Cyclic voltammetry was performed in a Vacuum Atmospheres Nexus II glovebox under a N_2 atmosphere using a CH Instruments model 620D or 660C potentiostat in THF using 0.2 M $[NBu_4][B(C_6F_5)_4]$ as the supporting electrolyte. Measurements were performed using a standard three-electrode cell containing a 1 mm PEEK-encased glassy carbon working electrode, Cypress Systems EE040, a 3 mm glassy carbon rod (Alfa) as the counter electrode, and a silver wire suspended in electrolyte solution and separated from the analyte solution by a Vycor frit (CH Instruments 112) as the pseudoreference electrode. Prior to the acquisition of each voltammogram, the working electrode was polished using 0.1 μm γ-alumina (BAS CF-1050) and rinsed with THF. Decamethylferrocene was used as an internal reference, and all potentials are reported versus the ferrocenium/ferrocene couple at 0.0 V. Low-temperature voltammetry experiments were performed in an o-xylene (-24 °C) slush bath in a glovebox coldwell. In situ IR experiments were recorded on a Mettler-Toledo ReactIR 15 FTIR spectrometer equipped with an MCT detector, connected to a 1.5 m AgX Fiber DS series (9.5 mm × 203 mm) probe with a silicon sensor. Experiments were performed in a 5 mL two-neck pear-shaped flask under a dinitrogen atmosphere using Schlenk line techniques. Typical

reactions contain ~0.03 M iron complex in a volume of 1−2 mL solvent. IR spectra were collected in intervals of 15 s in the normal collection mode or in "rapid collect" mode at a rate of five scans per second. Complexes $[3(CO)]^+$ and $[1(CO)]^+$ were prepared according to literature procedures.[22a]

$FeBr_2(P^{Et}N^{Me}P^{Et})(dmpm)$ (2(Br)). A similar procedure to the previously reported procedure for $FeCl_2(P^{Et}N^{Me}P^{Et})(dmpm)$ was used, where $FeBr_2$ was used in place of $FeCl_2$.[22a] $2(Br)$ was isolated as yellowish-green colored crystals (see Supporting Information for structural data). Yield: 82%. The paramagnetism of $2(Br)$ resulted in broad resonances in the ^1H NMR spectrum, which were uninformative, and there were no resonances in the ^{31}P NMR spectrum. Anal. Calcd for $C_{16}H_{41}Br_2FeNP_4$: C, 32.73; H, 7.04; N, 2.39. Found C, 32.78; H, 6.95; N, 2.44.

$FeHBr(P^{Et}N^{Me}P^{Et})(dmpm)$ (2(H)). A similar procedure to the previously reported procedure for $FeHCl(P^{Et}N^{Me}P^{Et})(dmpm)$ was used, where $FeBr_2(P^{Et}N^{Me}P^{Et})(dmpm)$ was used in place of $FeCl_2(P^{Et}N^{Me}P^{Et})(dmpm)$.[22a] $2(H)$ was isolated as feathery orange colored crystals (see Supporting Information for structural data). Yield: 48%. ^1H NMR (500 MHz, CD_2Cl_2): -27.03 (pentet, $^2J_{HP} = 48.2$ Hz, 1H), 1.00 (m, 6H, dmpm-P(CH_3)$_2$), 1.07 (m, 6H, dmpm-P(CH_3)$_2$), 1.35 (m, 4H, P(CH_2CH_3)$_2$), 1.43 (m, 6H, $P^{Et}N^{Me}P^{Et}$-P(CH_2CH_3)$_2$), 1.63 (m, 6H, $P^{Et}N^{Me}P^{Et}$-P(CH_2CH_3)$_2$), 1.67 (m, 4H, $P^{Et}N^{Me}P^{Et}$-P(CH_2CH_3)$_2$), 1.95 (m, 2H, $Et_2PCH_2NMeCH_2PEt_2$), 2.34 (s, 3H, N—CH_3), 2.68 (m, 2H, $Et_2PCH_2NMeCH_2PEt_2$), 3.01 (m, 1H, $Me_2PCH_2PMe_2$), 3.31 (m, 1H, $Me_2PCH_2PMe_2$). $^{31}P\{^1H\}$ NMR (202 MHz, THF-d_8): 0.61 (m, 2P, dmpm), 45.44 (m, 2P, $P^{Et}N^{Me}P^{Et}$). Anal. Calcd for $C_{16}H_{42}BrFeNP_4\cdot1/4OC_4H_8$: C, 38.80; H, 8.43; N, 2.66. Found C, 38.68; H, 8.44; N, 2.83.

$[Fe(N_2)Cl(P^{Et}N^{Me}P^{Et})(dmpm)]B(C_6F_5)_4$ ($[1(N_2)]B(C_6F_5)_4$). A 1 mL fluorobenzene solution of 10 mg (0.020 mmol) of $FeCl_2(P^{Et}N^{Me}P^{Et})$-(dmpm) was treated with 14.5 mg (0.020 mmol) of $KB(C_6F_5)_4$ in 0.25 mL of fluorobenzene. A pinkish-red solution resulted after stirring for 2 min. These solutions were used subsequently in protonation studies. IR (fluorobenzene): 2111 cm^{-1} (Fe—N_2).

$[FeBr(P^{Et}N^{Me}P^{Et})(dmpm)]B(C_6F_5)_4$. A 5 mL fluorobenzene solution of 30 mg (0.06 mmol) of $FeBr_2(P^{Et}N^{Me}P^{Et})(dmpm)$ was treated with 44.0 mg (0.06 mmol) of $KB(C_6F_5)_4$ in 5 mL of fluorobenzene. A pinkish-red solution resulted after stirring for 2 h. The reaction mixture was filtered and concentrated to about 1 mL. Red crystals were grown by vapor diffusion of pentane into a fluorobenzene solution. Yield: 42 mg (63%). Anal. Calcd for $C_{40}H_{41}BBrF_{20}FeNP_4\cdot C_6H_5F$: C, 43.09; H, 3.62; N, 1.09. Found C, 43.44; H, 3.46; N, 1.32.

$[Fe(N_2)Br(P^{Et}N^{Me}P^{Et})(dmpm)]B(C_6F_5)_4$ ($[2(N_2)]B(C_6F_5)_4$). A 1 mL fluorobenzene solution of 10 mg (0.017 mmol) of $FeBr_2(P^{Et}N^{Me}P^{Et})$-(dmpm) was treated with 12.3 mg (0.017 mmol) of $KB(C_6F_5)_4$ in 0.25 mL of fluorobenzene. A pinkish-red solution resulted after stirring for 2 min. These solutions were used subsequently in protonation studies. IR (fluorobenzene): 2110 cm^{-1} (Fe—N_2).

$[FeCl(CO)(P^{Et}N^{Me}P^{Et})(dmpm)]BPh_4$ ($[1(CO)]B(C_6F_5)_4$). A 5 mL THF solution of 50 mg (0.10 mmol) of $FeCl_2(P^{Et}N^{Me}P^{Et})(dmpm)$ was treated with 36 mg (0.11 mmol) of $NaBPh_4$ in 5 mL THF. The resulting orange-red solution was treated with a light bubbling of CO (1 atm), immediately resulting in a yellow solution. The solution was filtered, and the solvent was removed under reduced pressure. X-ray quality crystals were grown from vapor diffusion of pentane into a THF solution (see Supporting Information for structural data). The IR characterization data were found to match $[FeCl(CO)(P^{Et}N^{Me}P^{Et})$-(dmpm)]$_2FeCl_4$, which was previously reported by DuBois and co-workers.[22a]

$[FeBr(CO)(P^{Et}N^{Me}P^{Et})(dmpm)]BPh_4$ ($[2(CO)]B(C_6F_5)_4$). A 5 mL THF solution of 40 mg (0.07 mmol) of $FeBr_2(P^{Et}N^{Me}P^{Et})(dmpm)$ was treated with 24 mg (0.07 mmol) of $NaBPh_4$ in 5 mL of THF. The resulting yellow solution was treated with a light bubbling of a CO atmosphere, immediately resulting in a yellowish-orange color. The solution was filtered, and the solvent was removed under reduced pressure. X-ray quality yellow crystals were grown from vapor diffusion of pentane into a THF solution (see Supporting Information for structural data). Yield: 36 mg (60%). ^1H NMR (500 MHz, CD_2Cl_2):

1.00–1.29 (m, 12H, dmpm-P(CH$_3$)$_2$), 1.34–2.22 (m, 20H, P-(CH$_2$CH$_3$)$_2$), 1.52 (s, 3H, N–CH$_3$), 2.43 (s, 3H, Fe–NH$_3$), 2.89 (m, 2H, Et$_2$PCH$_2$NMeCH$_2$PEt$_2$), 3.17 (m, 2H, Et$_2$PCH$_2$NMeCH$_2$PEt$_2$), 3.49 (m, 2H, Me$_2$PCH$_2$PMe$_2$), 7.30–7.47 (m, 20H, BPh$_4$). ^{31}P NMR (202 MHz, CD$_2$Cl$_2$): −12.2 (m, 2P, dmpm), 25.8 (m, 2P, P^{Et}N^{Me}P^{Et}). IR (fluorobenzene) 1946 cm^{-1}.

[FeH(N$_2$)(P^{Et}N^{Me}P^{Et})(dmpm)]BPh$_4$ ([3(N$_2$)]BPh$_4$). A 5 mL THF solution of 31 mg (0.065 mmol) of FeHCl(P^{Et}N^{Me}P^{Et})(dmpm) was treated with 22 mg (0.063 mmol) of NaBPh$_4$ in 5 mL of THF. A yellow solution resulted after stirring for 20 h. The cloudy yellow solution was filtered and recrystallized from a vapor diffusion of pentane into a THF solution, resulting in yellow crystals. Yield: 37 mg (75%). ^{1}H NMR (500 MHz, THF-d_8): −14.53 (dt, $^2J_{PH}$ = 95.7, 47.9 Hz, 1H, Fe-H), 1.15 (m, 12H, dmpm-P(CH$_3$)$_2$), 1.43 (m, 4H, P(CH$_2$CH$_3$)$_2$), 1.60 (m, 6H, P(CH$_2$CH$_3$)$_2$), 1.72 (m, 6H, P-(CH$_2$CH$_3$)$_2$), 1.83 (m, 4H, P(CH$_2$CH$_3$)$_2$), 2.41 (s, 3H, N–CH$_3$), 2.47 (m, 2H, Et$_2$PCH$_2$NMeCH$_2$PEt$_2$), 3.00 (m, 2H, Et$_2$PCH$_2$NMeCH$_2$PEt$_2$), 3.22 (m, 2H, dmpm-Me$_2$PCH$_2$PMe$_2$), 6.71 (t, 4H, $^3J_{HH}$ = 6.8 Hz, p-phenyl protons of BPh$_4$), 6.86 (t, 8H, $^3J_{HH}$ = 7.8 Hz, o-phenyl protons of BPh$_4$), 7.28 (m, 8H, m-phenyl protons of BPh$_4$). ^{31}P{^{1}H} NMR (202 MHz, THF-d_8): 4.55 (m, 2P, dmpm), 44.88 (m, 2P, P^{Et}N^{Me}P^{Et}). ^{15}N{^{1}H} NMR (51 MHz, THF-d_8) −41.75 (s, Fe–N$_\alpha$≡N$_\beta$), −59.80 (s, Fe-N$_\alpha$≡N$_\beta$), −361.82 (t, $^2J_{NP}$ = 13.5 Hz, P^{Et}N^{Me}P^{Et}). Anal. Calcd for C$_{40}$H$_{62}$BFeN$_3$P$_4$: C, 61.95; H, 8.06; N, 5.42. Found C, 61.73; H, 7.87; N, 5.23.

In Situ Protonation of [1(N$_2$)]B(C$_6$F$_5$)$_4$, [2(N$_2$)]B(C$_6$F$_5$)$_4$, and [3(N$_2$)]B(C$_6$F$_5$)$_4$. A 1.0 mL fluorobenzene solution of 10 mg (∼ 0.015 mmol) of **1(Cl)**, **2(Br)**, or **1(H)** was treated with 11 mg (∼ 0.015 mol) of KB(C$_6$F$_5$)$_4$ in 1.0 mL of fluorobenzene. A yellow (complex [3(N$_2$)]B(C$_6$F$_5$)$_4$) or pinkish-red (complexes [1(N$_2$)]B(C$_6$F$_5$)$_4$ and [2(N$_2$)]B(C$_6$F$_5$)$_4$) solution resulted after stirring for 2 min. After this time, the ReactIR probe was inserted into the reaction mixture. The solution was cooled in an acetonitrile slush bath (−45 °C) and stirred for 30 min for the temperature to equilibrate. The addition of 0.5 mL of 0.045 M [H(OEt$_2$)$_2$][B(C$_6$F$_5$)$_4$] in fluorobenzene resulted in a slight darkening of the solution. The solution was stirred for 30 min; then 10 μL (0.045 mmol) Et$_3$N was added and the solution was stirred for 30 min.

In Situ Protonation of [1(CO)]B(C$_6$F$_5$)$_4$, [2(CO)]B(C$_6$F$_5$)$_4$, [3(CO)]B(C$_6$F$_5$)$_4$. The same procedure as described for the in situ protonation of [1(N$_2$)]B(C$_6$F$_5$)$_4$, [2(N$_2$)]B(C$_6$F$_5$)$_4$, and [3(N$_2$)]B-(C$_6$F$_5$)$_4$ was used, except that the solutions were treated with CO (1 atm) for 30 min before the acid addition. The acid and base additions were undertaken at 25 °C, as the protonated CO complexes were not temperature-sensitive, unlike the N$_2$ complexes described above.

[FeH(^{15}NH$_3$)(P^{Et}N^{Me}P^{Et})(dmpm)]B(C$_6$F$_5$)$_4$ ([3(^{15}NH$_3$)]B(C$_6$F$_5$)$_4$). A 1.0 mL THF-d_8 solution of 10 mg (∼ 0.015 mmol) of [3(N$_2$)]B(C$_6$F$_5$)$_4$ was treated with 1 atm of ^{15}NH$_3$. A bright yellow solution resulted after 30 min. Complete conversion to [3(NH$_3$)]$^+$ was observed to occur after 5 h. ^{1}H NMR (500 MHz, THF-d_8): −25.0 (pentet, $^2J_{PH}$ = 46.2 Hz, 1H, Fe-H), 1.00–1.25 (m, 12H, dmpm-P(CH$_3$)$_2$), 1.40–2.1 (m, 20H, P(CH$_2$CH$_3$)$_2$), 1.52 (s, 3H, N–CH$_3$), 1.60 (br s, 3H, Fe–NH$_3$), 2.39 (m, 2H, Et$_2$PCH$_2$NMeCH$_2$PEt$_2$), 2.69 (m, 2H, Et$_2$PCH$_2$NMeCH$_2$PEt$_2$), 3.04 (m, 1H, Me$_2$PCH$_2$PMe$_2$), 3.25 (m, 1H, Me$_2$PCH$_2$PMe$_2$). ^{31}P{^{1}H} NMR (202 MHz, THF-d_8): 2.6 (m, 2P, dmpm), 47.9 (m, 2P, P^{Et}N^{Me}P^{Et}). ^{15}N{^{1}H} NMR (51 MHz, THF-d_8) −356.2 (t, $^2J_{NP}$ = 12.9 Hz, P^{Et}N^{Me}P^{Et}), −433.1 (s, NH$_3$).

HFe(Et$_2$PC(H)N(Me)CH$_2$PEt$_2$)(P^{Et}N^{Me}P^{Et}) (4). A 15 mL THF slurry of 265 mg (1.23 mmol) of FeBr$_2$ and 575 mg (2.44 mmol) of P^{Et}N^{Me}P^{Et} was treated with 550 mg (22.6 mmol) of Mg powder. The blackish-gray slurry was stirred for 20 h. The solvent was removed under reduced pressure, and the residue was extracted with pentane. X-ray quality crystals were grown from hexamethyldisiloxane solutions at −30 °C. Yield: 249 mg (39%). ^{1}H NMR (500 MHz, THF-d_8): −13.86 (m, 1H, Fe-H), 0.91–1.94 (40H, PEt), 2.21–2.99 (6H, Et$_2$PCH$_2$NMeCH$_2$PEt$_2$), 2.25 (s, 3H, N–CH$_3$), 2.52 (s, 3H, N–CH$_3$), 3.43 (br s, 1H, Fe–CH). ^{31}P{^{1}H} NMR (202 MHz, THF-d_8): 14.9 (m, 1P, P trans to hydride), 40.6 (dt, 1P, $^2J_{PP}$ = 22, 57 Hz, P adjacent to CH activated methylene), 53.2 (dd, 1P, $^2J_{PP}$ = 36, 57 Hz, P trans to CH activated methylene), 72.6 (dd, 1P, $^2J_{PP}$ = 22, 36 Hz, P closest to

FeH). IR (KBr): 1900 cm^{-1} (Fe−H). Anal. Calcd for C$_{22}$H$_{54}$FeN$_2$P$_4$·Me$_3$SiOSiMe$_3$: C, 48.78; H, 10.31; N, 4.55. Found C, 48.33; H, 9.90; N, 5.10.

[H(OEt$_2$)$_2$][B(C$_6$F$_5$)$_4$]. Ether (400 mL) was added to KB(C$_6$F$_5$)$_4$ (25.29 g, 35.22 mmol), giving a cloudy off-white suspension. HCl (2 M in diethyl ether, 20 mL) was added via syringe over 5 min, and the mixture was stirred overnight. Volatile components were removed under reduced pressure, affording an oily solid. Ether (50 mL) was added, and the volatiles were again removed, giving a clumpy off-white solid. The solids were extracted with fluorobenzene (300 mL), then filtered through Celite, and then through a syringe filter to give a clear, pale brown-yellow solution. Pentane (300 mL) was added, and the resulting off-white precipitate was collected with a medium porosity frit and extracted with fluorobenzene (70 mL). The resulting pale brown-yellow solution was layered with pentane (250 mL), affording clear/colorless crystals after 24 h. The crystals were collected, rinsed with pentane, and dried under a vacuum. Yield: 18.19 g (62%). Spectroscopic analysis matched the previously reported data.[44]

Theoretical Calculations. All structures were fully optimized without symmetry constraints using the B3P86[45] functional as implemented in Gaussian 09.[46] The Stuttgart basis set with effective core potential (ECP)[47] was used for the Fe atom, and the 6-31G** basis set[48] was used for other nonmetal atoms. Each stationary point was confirmed by frequency calculation at the same level of theory to be a real local minimum on the potential energy surface without imaginary frequency. All reported free energies are for THF solution at the standard state (T = 298 K, P = 1 atm of N$_2$, 1 mol/L concentration of all species in THF) as modeled by a polarized continuum model (C-PCM)[49] with standard correction for (harmonic) vibrational, rotational, and translational thermal free energy contributions. All calculated proton affinities and pK_a values are for THF solutions and are calculated relative to the value of Et$_3$NH$^+$ (pK_a = 12.5),[50] which is assigned its experimental value to anchor the calculated pK_a scale.

X-Ray Diffraction Studies. X-ray diffraction data were collected on a Bruker-AXS Kappa APEX II CCD diffractometer with 0.71073 Å Mo Kα radiation. Selected crystals were mounted using NVH immersion oil onto a nylon fiber and cooled to the data collection temperature of 100−120 K. Unit cell parameters were obtained from 60 data frames, 0.5° Φ, from three different sections of the Ewald sphere. Cell parameters were retrieved using APEX II software[51] and refined using SAINT+[52] on all observed reflections. Each data set was treated with SADABS[53] absorption corrections based on redundant multiscan data. The structure was solved by direct methods and refined with the least-squares method on F^2 using the SHELXTL program package.[54] Crystallographic data for each structure and details regarding specific solution refinement for each compound are provided in the Supporting Information.

■ ASSOCIATED CONTENT

⑤ Supporting Information

ReactIR plots showing the reactivity of [3(N$_2$)]B(C$_6$F$_5$)$_4$ with CO and [1(CO)]BPh$_4$ and [2(CO)]BPh$_4$ with protons; molecular structures of **1(Cl)**, **2(Br)**, **2(H)**, [1(CO)]BPh$_4$, [2(CO)]BPh$_4$, and [3(NH$_3$)]B(C$_6$F$_5$)$_4$; experimental details of X-ray diffraction studies; ^{15}N NMR of [3(N$_2$)]$^+$; multinuclear NMR spectra of acid addition to [3(N$_2$)]$^+$; scan rate dependence on the CV of [3(N$_2$)]BPh$_4$; frontier molecular orbitals of [3(N$_2$)]$^+$ and [1(N$_2$)]$^+$; NBO analysis of Fe complexes; charge model for N$_2$ bond polarization; and coordinates for optimized structures. This material is available free of charge via the Internet at http://pubs.acs.org.

■ AUTHOR INFORMATION

Corresponding Author
*E-mail: Michael.Mock@pnnl.gov.

Notes

The authors declare no competing financial interest.

■ REFERENCES

(1) (a) Hinrichsen, S.; Broda, H.; Gradert, C.; Soncksen, L.; Tuczek, F. *Annu. Rep. Prog. Chem., Sect. A* **2012**, *108*, 17−47. (b) Nishibayashi, Y. *Dalton Trans.* **2012**, *41*, 7447−7453. (c) MacKay, B. A.; Fryzuk, M. D. *Chem. Rev.* **2004**, *104*, 385−401. (d) Fryzuk, M. D.; Johnson, S. A. *Coord. Chem. Rev.* **2000**, *200−202*, 379−409.

(2) (a) Hazari, N. *Chem. Soc. Rev.* **2010**, *39*, 4044−4056. (b) Crossland, J. L.; Tyler, D. R. *Coord. Chem. Rev.* **2010**, *254*, 1883−1894.

(3) Enthaler, S.; Junge, K.; Beller, M. *Angew. Chem., Int. Ed. Engl.* **2008**, *47*, 3317−3321.

(4) (a) Lancaster, K. M.; Roemelt, M.; Ettenhuber, P.; Hu, Y.; Ribbe, M. W.; Neese, F.; Bergmann, U.; DeBeer, S. *Science* **2011**, *334*, 974−977. (b) Spatzal, T.; Aksoyoglu, M.; Zhang, L.; Andrade, S. L. A.; Schleicher, E.; Weber, S.; Rees, D. C.; Einsle, O. *Science* **2011**, *334*, 940−940. (c) Ramaswamy, S. *Science* **2011**, *334*, 914−915. (d) Eady, R. R. *Chem. Rev.* **1996**, *96*, 3013−3030. (e) Burgess, B. K.; Lowe, D. J. *Chem. Rev.* **1996**, *96*, 2983−3011.

(5) (a) Dance, I. *Dalton Trans.* **2012**, *41*, 7647−7659. (b) Sellmann, D.; Sutter, J. *Acc. Chem. Res.* **1997**, *30*, 460−469. (c) Sellmann, D.; Sutter, J. *J. Biol. Inorg. Chem.* **1996**, *1*, 587−593.

(6) (a) Dance, I. *Chem. Commun.* **1997**, 165−166. (b) Dance, I. *Dalton Trans.* **2008**, 5977−5991. (c) Chatt, J.; Dilworth, J. R.; Richards, R. L. *Chem. Rev.* **1978**, *78*, 589−625.

(7) (a) Lukoyanov, D.; Yang, Z.-Y.; Barney, B. M.; Dean, D. R.; Seefeldt, L. C.; Hoffman, B. M. *Proc. Natl. Acad. Sci. U. S. A.* **2012**, *109*, 5583−5587. (b) Lukoyanov, D.; Dikanov, S. A.; Yang, Z.-Y.; Barney, B. M.; Samoilova, R. I.; Narasimhulu, K. V.; Dean, D. R.; Seefeldt, L. C.; Hoffman, B. M. *J. Am. Chem. Soc.* **2011**, *133*, 11655−11664. (c) Seefeldt, L. C.; Hoffman, B. M.; Dean, D. R. *Annu. Rev. Biochem.* **2009**, *78*, 701−722. (d) Barney, B. M.; Lee, H.-I.; Dos, S. P. C.; Hoffman, B. M.; Dean, D. R.; Seefeldt, L. C. *Dalton Trans.* **2006**, 2277−2284. (e) Hoffman, B. M.; Lukoyanov, D.; Dean, D. R.; Seefeldt, L. C. *Acc. Chem. Res.* **2013**, *46*, 587−595.

(8) (a) Schrock, R. R. *Acc. Chem. Res.* **2005**, *38*, 955−962. (b) Schrock, R. R. Catalytic reduction of dinitrogen to ammonia by molybdenum. In *Catalysis without Precious Metals*; Bullock, R. M., Ed.; Wiley-Blackwell: Weinheim, Germany, 2010; pp 25−50. (c) Yandulov, D. V.; Schrock, R. R. *Science* **2003**, *301*, 76−78.

(9) (a) Arashiba, K.; Miyake, Y.; Nishibayashi, Y. *Nat. Chem.* **2011**, *3*, 120−125. (b) Kinoshita, E.; Arashiba, K.; Kuriyama, S.; Miyake, Y.; Shimazaki, R.; Nakanishi, H.; Nishibayashi, Y. *Organometallics* **2012**, *31*, 8437−8443.

(10) Yuki, M.; Tanaka, H.; Sasaki, K.; Miyake, Y.; Yoshizawa, K.; Nishibayashi, Y. *Nat. Commun.* **2012**, *3*, 1254.

(11) (a) Leigh, G. J.; Jimenez-Tenorio, M. *J. Am. Chem. Soc.* **1991**, *113*, 5862−5863. (b) Hills, A.; Hughes, D. L.; Jimenez-Tenorio, M.; Leigh, G. J.; Rowley, A. T. *J. Chem. Soc., Dalton Trans.* **1993**, 3041−3049.

(12) Rodriguez, M. M.; Bill, E.; Brennessel, W. W.; Holland, P. L. *Science* **2011**, *334*, 780−783.

(13) Gilbertson, J. D.; Szymczak, N. K.; Tyler, D. R. *J. Am. Chem. Soc.* **2005**, *127*, 10184−10185.

(14) (a) Smith, J. M.; Subedi, D. *Dalton Trans.* **2012**, *41*, 1423−1429. (b) Scepaniak, J. J.; Young, J. A.; Bontchev, R. P.; Smith, J. M. *Angew. Chem., Int. Ed. Engl.* **2009**, *48*, 3158−3160.

(15) Mankad, N. P.; Whited, M. T.; Peters, J. C. *Angew. Chem., Int. Ed.* **2007**, *46*, 5768−5771.

(16) (a) Dilworth, M. J.; Fisher, K.; Kim, C.-H.; Newton, W. E. *Biochemistry* **1998**, *37*, 17495−17505. (b) Barton, B. E.; Olsen, M. T.; Rauchfuss, T. B. *J. Am. Chem. Soc.* **2008**, *130*, 16834−16835. (c) Silakov, A.; Wenk, B.; Reijerse, E.; Lubitz, W. *Phys. Chem. Chem. Phys.* **2009**, *11*, 6592−6599. (d) Erdem, Ö. F.; Schwartz, L.; Stein, M.; Silakov, A.; Kaur-Ghumaan, S.; Huang, P.; Ott, S.; Reijerse, E. J.; Lubitz, W. *Angew. Chem., Int. Ed. Engl.* **2011**, *50*, 1439−1443.

(17) Dance, I. *Dalton Trans.* **2008**, *37*, 5992−5998.

(18) (a) Weinberg, D. R.; Gagliardi, C. J.; Hull, J. F.; Murphy, C. F.; Kent, C. A.; Westlake, B. C.; Paul, A.; Ess, D. H.; McCafferty, D. G.; Meyer, T. J. *Chem. Rev.* **2012**, *112*, 4016−4093. (b) Huynh, M. H. V.; Meyer, T. J. *Chem. Rev.* **2007**, *107*, 5004−5064. (c) Warren, J. J.; Tronic, T. A.; Mayer, J. M. *Chem. Rev.* **2010**, *110*, 6961−7001.

(19) (a) DuBois, D. L.; Bullock, R. M. *Eur. J. Inorg. Chem.* **2011**, *2011*, 1017−1027. (b) Kilgore, U. J.; Stewart, M. P.; Helm, M. L.; Dougherty, W. G.; Kassel, W. S.; DuBois, M. R.; DuBois, D. L.; Bullock, R. M. *Inorg. Chem.* **2011**, *50*, 10908−10918. (c) Kilgore, U. J.; Roberts, J. A. S.; Pool, D. H.; Appel, A. M.; Stewart, M. P.; DuBois, M. R.; Dougherty, W. G.; Kassel, W. S.; Bullock, R. M.; DuBois, D. L. *J. Am. Chem. Soc.* **2011**, *133*, 5861−5872.

(20) (a) Tronic, T. A.; Kaminsky, W.; Coggins, M. K.; Mayer, J. M. *Inorg. Chem.* **2012**, *51*, 10916−10928. (b) Matson, B. D.; Carver, C. T.; Von Ruden, A.; Yang, J. Y.; Raugei, S.; Mayer, J. M. *Chem. Commun.* **2012**, *48*, 11100−11102. (c) Carver, C. T.; Matson, B. D.; Mayer, J. M. *J. Am. Chem. Soc.* **2012**, *134*, 5444−5447.

(21) (a) Weiss, C. J.; Groves, A. N.; Mock, M. T.; Dougherty, W. G.; Kassel, W. S.; Helm, M. L.; DuBois, D. L.; Bullock, R. M. *Dalton Trans.* **2012**, *41*, 4517−4529. (b) Mock, M. T.; Chen, S.; Rousseau, R.; O'Hagan, M. J.; Dougherty, W. G.; Kassel, W. S.; DuBois, D. L.; Bullock, R. M. *Chem. Commun.* **2011**, *47*, 12212−12214.

(22) (a) Henry, R. M.; Shoemaker, R. K.; Newell, R. H.; Jacobsen, G. M.; DuBois, D. L.; DuBois, M. R. *Organometallics* **2005**, *24*, 2481−2491. (b) Henry, R. M.; Shoemaker, R. K.; DuBois, D. L.; DuBois, M. R. *J. Am. Chem. Soc.* **2006**, *128*, 3002−3010. (c) Attempts to synthesize $FeCl_2(P^{Et}N^{Me}P^{Et})(dmpe)$ (dmpe = $Me_2PCH_2CH_2PMe_2$), resulted in only $FeCl_2(dmpe)_2$, $FeCl_2(P^{Et}N^{Me}P^{Et})$, and $P^{Et}N^{Me}P^{Et}$; thus dmpm was chosen as the second bidentate phosphine.

(23) Hills, A.; Hughes, D. L.; Jimenez-Tenorio, M.; Leigh, G. J. *J. Organomet. Chem.* **1990**, *391*, C41−C44.

(24) Crossland, J. L.; Young, D. M.; Zakharov, L. N.; Tyler, D. R. *Dalton Trans.* **2009**, 9253−9259.

(25) Bau, R.; Teller, R. G.; Kirtley, S. W.; Koetzle, T. F. *Acc. Chem. Res.* **1979**, *12*, 176−183.

(26) Buys, I. E.; Field, L. D.; Hambley, T. W.; McQueen, A. E. D. *Acta Crystallogr., Sect. C: Cryst. Struct. Commun.* **1993**, *C49*, 1056−1059.

(27) Wiesler, B. E.; Lehnert, N.; Tuczek, F.; Neuhausen, J.; Tremel, W. *Angew. Chem., Int. Ed.* **1998**, *37*, 815−817.

(28) Franke, O.; Wiesler, B. E.; Lehnert, N.; Nather, C.; Ksenofontov, V.; Neuhausen, J.; Tuczek, F. *Inorg. Chem.* **2002**, *41*, 3491−3499.

(29) Mason, J. *Chem. Rev.* **1981**, *81*, 205−227.

(30) Yelle, R. B.; Crossland, J. L.; Szymczak, N. K.; Tyler, D. R. *Inorg. Chem.* **2009**, *48*, 861−871.

(31) Kinney, R. A.; McNaughton, R. L.; Chin, J. M.; Schrock, R. R.; Hoffman, B. M. *Inorg. Chem.* **2011**, *50*, 418−420.

(32) (a) Stanley, J. L.; Heiden, Z. M.; Rauchfuss, T. B.; Wilson, S. R. *Organometallics* **2008**, *27*, 119−125. (b) Carroll, M. E.; Barton, B. E.; Rauchfuss, T. B.; Carroll, P. J. *J. Am. Chem. Soc.* **2012**, *134*, 18843−18852. (c) Schwartz, L.; Eilers, G.; Eriksson, L.; Gogoll, A.; Lomoth, R.; Ott, S. *Chem. Commun.* **2006**, 520−522. (d) Ott, S.; Kritikos, M.; Akermark, B.; Sun, L.; Lomoth, R. *Angew. Chem.; Int. Ed. Engl.* **2004**, *43*, 1006−1009. (e) Lawrence, J. D.; Li, H.; Rauchfuss, T. B.; Benard, M.; Rohmer, M.-M. *Angew. Chem., Int. Ed. Engl.* **2001**, *40*, 1768−1771.

(33) Gao, Y.; Holah, D. G.; Hughes, A. N.; Spivak, G. J.; Havighurst, M. D.; Magnuson, V. R.; Polyakov, V. *Polyhedron* **1997**, *16*, 2797−2807.

(34) Fox, D. J.; Bergman, R. G. *Organometallics* **2004**, *23*, 1656−1670.

(35) Field, L. D.; Li, H. L.; Dalgarno, S. J.; Jensen, P.; McIntosh, R. D. *Inorg. Chem.* **2011**, *50*, 5468−5476.

(36) Crossland, J. L.; Balesdent, C. G.; Tyler, D. R. *Inorg. Chem.* **2012**, *51*, 439−445.

(37) (a) Sellmann, D.; Soglowek, W.; Knoch, F.; Ritter, G.; Dengler, J. *Inorg. Chem.* **1992**, *31*, 3711−3717. (b) Chetcuti, P. A.; Liégard, A.; Rihs, G.; Rist, G.; Schweiger, A. *Helv. Chim. Acta* **1991**, *74*, 1591−1599. (c) Bowman, A. C.; Bart, S. C.; Heinemann, F. W.; Meyer, K.; Chirik, P. J. *Inorg. Chem.* **2009**, *48*, 5587−5589. (d) Vela, J.; Stoian, S.; Flaschenriem, C. J.; Münck, E.; Holland, P. L. *J. Am. Chem. Soc.* **2004**, *126*, 4522−4523. (e) Lee, Y.; Mankad, N. P.; Peters, J. C. *Nat. Chem.* **2010**, *2*, 558−565.

(38) (a) Henderson, R. A. *J. Chem. Soc., Dalton Trans.* **1988**, 515. (b) Franke, O.; Wiesler, B. E.; Lehnert, N.; Peters, G.; Burger, P.; Tuczek, F. *Z. Anorg. Allg. Chem.* **2006**, *632*, 1247−1256. (c) Tuczek, F.; Lehnert, N. *Angew. Chem., Int. Ed. Engl.* **1998**, *37*, 2636−2638.

(39) Karsch, H. H.; Neugebauer, D. *Angew. Chem., Int. Ed.* **1982**, *21*, 312−313.

(40) Hirano, M.; Akita, M.; Morikita, T.; Kubo, H.; Fukuoka, A.; Komiya, S. *J. Chem. Soc., Dalton Trans.* **1997**, 3453−3458.

(41) (a) Reed, A. E.; Curtiss, L. A.; Weinhold, F. *Chem. Rev.* **1988**, *88*, 899−926. (b) Foster, J. P.; Weinhold, F. *J. Am. Chem. Soc.* **1980**, *102*, 7211−7218.

(42) Curtis, C. J.; Miedaner, A.; Ciancanelli, R.; Ellis, W. W.; Noll, B. C.; Rakowski DuBois, M.; DuBois, D. L. *Inorg. Chem.* **2003**, *42*, 216−227.

(43) LeSuer, R. J.; Geiger, W. E. *Angew. Chem., Int. Ed. Engl.* **2000**, *39*, 248−250.

(44) Rach, S. F.; Herdtweck, E.; Kühn, F. E. *J. Organomet. Chem.* **2011**, *696*, 1817−1823.

(45) (a) Becke, A. D. *J. Chem. Phys.* **1993**, *98*, 5648−5652. (b) Perdew, J. P. *Phys. Rev. B* **1986**, *33*, 8822−8824.

(46) Frisch, M. J.; Trucks, G. W.; Schlegel, H. B.; Scuseria, G. E.; Robb, M. A.; Cheeseman, J. R.; Scalmani, G.; Barone, V.; Mennucci, B.; Petersson, G. A.; Nakatsuji, H.; Caricato, M.; Li, X.; Hratchian, H. P.; Izmaylov, A. F.; Bloino, J.; Zheng, G.; Sonnenberg, J. L.; Hada, M.; Ehara, M.; Toyota, K.; Fukuda, R.; Hasegawa, J.; Ishida, M.; Nakajima, T.; Honda, Y.; Kitao, O.; Nakai, H.; Vreven, T.; Montgomery, J. A., Jr.; Peralta, J. E.; Ogliaro, F.; Bearpark, M.; Heyd, J. J.; Brothers, E.; Kudin, K. N.; Staroverov, V. N.; Kobayashi, R.; Normand, J.; Raghavachari, K.; Rendell, A.; Burant, J. C.; Iyengar, S. S.; Tomasi, J.; Cossi, M.; Rega, N.; Millam, N. J.; Klene, M.; Knox, J. E.; Cross, J. B.; Bakken, V.; Adamo, C.; Jaramillo, J.; Gomperts, R.; Stratmann, R. E.; Yazyev, O.; Austin, A. J.; Cammi, R.; Pomelli, C.; Ochterski, J. W.; Martin, R. L.; Morokuma, K.; Zakrzewski, V. G.; Voth, G. A.; Salvador, P.; Dannenberg, J. J.; Dapprich, S.; Daniels, A. D.; Farkas, Ö.; Foresman, J. B.; Ortiz, J. V.; Cioslowski, J.; Fox, D. J. *Gaussian 09*, revision A.1; Gaussian, Inc.: Wallingford, CT, 2009.

(47) Andrae, D.; Häußermann, U.; Dolg, M.; Stoll, H.; Preuß, H. *Theor. Chem. Acc.* **1990**, *77*, 123−141.

(48) (a) Francl, M. M.; Pietro, W. J.; Hehre, W. J.; Binkley, J. S.; Gordon, M. S.; DeFrees, D. J.; Pople, J. A. *J. Chem. Phys.* **1982**, *77*, 3654−3665. (b) Rassolov, V. A.; Ratner, M. A.; Pople, J. A.; Redfern, P. C.; Curtiss, L. A. *J. Comput. Chem.* **2001**, *22*, 976−984.

(49) Barone, V.; Cossi, M. *J. Phys. Chem. A* **1998**, *102*, 1995−2001.

(50) (a) Abdur-Rashid, K.; Fong, T. P.; Greaves, B.; Gusev, D. G.; Hinman, J. G.; Landau, S. E.; Lough, A. J.; Morris, R. H. *J. Am. Chem. Soc.* **2000**, *122*, 9155−9171. (b) Rodima, T.; Kaljurand, I.; Pihl, A.; Maemets, V.; Leito, I.; Koppel, I. *J. Org. Chem.* **2002**, *67*, 1873−1881.

(51) *APEX II*, v. 2009.3; Bruker AXS: Madison, WI, 2009.

(52) *SAINT+*, v. 7.56A; Bruker AXS: Madison, WI, 2009.

(53) *SADABS*, v. 2008/1; Bruker AXS Inc.: Madison, WI, 2008.

(54) Sheldrick, G. M. *SHELXTL*, v. 2008; Bruker AXS Inc.: Madison, WI, 2008.

4039

dx.doi.org/10.1021/ic4000704 | *Inorg. Chem.* 2013, 52, 4026−4039